NAVAL POSTGRADUATE SCHOOL
Monterey, California

THESIS

S635

MARINE BOUNDARY LAYER DEPTH AND RELATIVE HUMIDITY ESTIMATES USING MULTISPECTRAL SATELLITE MEASUREMENTS

by

Steven P. Smolinski

March 1988

Thesis Advisor P.A. Durkee

Approved for public release; distribution is unlimited.

T239247

Unclassified

security classification of this page

REPORT DOCUMENTATION PAGE

1a Report Security Classification: Unclassified		1b Restrictive Markings	
2a Security Classification Authority		3 Distribution Availability of Report: Approved for public release; distribution is unlimited.	
2b Declassification Downgrading Schedule			
4 Performing Organization Report Number(s)		5 Monitoring Organization Report Number(s)	
6a Name of Performing Organization: Naval Postgraduate School	6b Office Symbol (*if applicable*): 35	7a Name of Monitoring Organization: Naval Postgraduate School	
6c Address (*city, state, and ZIP code*): Monterey, CA 93943-5000		7b Address (*city, state, and ZIP code*): Monterey, CA 93943-5000	
8a Name of Funding Sponsoring Organization	8b Office Symbol (*if applicable*)	9 Procurement Instrument Identification Number	
8c Address (*city, state, and ZIP code*)		10 Source of Funding Numbers	
		Program Element No	Project No / Task No / Work Unit Accession No

11 Title (*Include security classification*): MARINE BOUNDARY LAYER DEPTH AND RELATIVE HUMIDITY ESTIMATES USING MULTISPECTRAL SATELLITE MEASUREMENTS

12 Personal Author(s): Steven P. Smolinski

13a Type of Report	13b Time Covered	14 Date of Report (*year, month, day*)	15 Page Count
Master's Thesis	From To	March 1988	81

16 Supplementary Notation: The views expressed in this thesis are those of the author and do not reflect the official policy or position of the Department of Defense or the U.S. Government.

17 Cosati Codes			18 Subject Terms (*continue on reverse if necessary and identify by block number*)
Field	Group	Subgroup	Satellite, Boundary Layer, Remote Sensing

19 Abstract (*continue on reverse if necessary and identify by block number*)

A technique is presented to estimate surface relative humidity and boundary layer depth from multispectral satellite measurements using the AVHRR sensor on TIROS-N generation satellites. A sensitivity study quantifies the effect of a combination of input measurement errors of sea-surface temperature, optical depth and total water vapor used in the technique to produce outputs of surface relative humidity and boundary layer depth under simulated conditions and model atmospheres. Technique verification is then accomplished with satellite data compared to ship and aircraft vertical soundings and sea-surface temperature measurements. The root mean square differences between the surface relative humidity/boundary layer depth satellite-measured estimates and verified measurements are 6% and 75 m respectively. Finally, synoptic-scale mapping of the surface relative humidity and boundary layer depth fields based on the satellite derived estimates is accomplished with monochromatic and color enhanced satellite images. Horizontal variability of surface relative humidity and boundary layer depth on the order of kilometers can be visually detected from these images.

20 Distribution Availability of Abstract	21 Abstract Security Classification	
☒ unclassified unlimited ☐ same as report ☐ DTIC users	Unclassified	
22a Name of Responsible Individual: P.A. Durkee	22b Telephone (*include Area code*): (408) 646-3465	22c Office Symbol: 63De

DD FORM 1473,84 MAR

83 APR edition may be used until exhausted
All other editions are obsolete

security classification of this page

Unclassified

Approved for public release; distribution is unlimited.

Marine Boundary Layer Depth and Relative Humidity Estimates Using Multispectral Satellite Measurements

by

Steven P. Smolinski
Lieutenant Commander, United States Navy
B.A., University of Virginia, 1978

Submitted in partial fulfillment of the
requirements for the degree of

MASTER OF SCIENCE IN METEOROLOGY AND OCEANOGRAPHY

from the

NAVAL POSTGRADUATE SCHOOL
March 1988

ABSTRACT

A technique is presented to estimate surface relative humidity and boundary layer depth from multispectral satellite measurements using the AVHRR sensor on TIROS-N generation satellites. A sensitivity study quantifies the effect of a combination of input measurement errors of sea-surface temperature, optical depth and total water vapor used in the technique to produce outputs of surface relative humidity and boundary layer depth under simulated conditions and model atmospheres. Technique verification is then accomplished with satellite data compared to ship and aircraft vertical soundings and sea-surface temperature measurements. The root mean square differences between the surface relative humidity/boundary layer depth satellite-measured estimates and verified measurements are 6% and 75 m respectively. Finally, synoptic-scale mapping of the surface relative humidity and boundary layer depth fields based on the satellite derived estimates is accomplished with monochromatic and color enhanced satellite images. Horizontal variability of surface relative humidity and boundary layer depth on the order of kilometers can be visually detected from these images.

TABLE OF CONTENTS

I. INTRODUCTION 1

II. THEORETICAL BACKGROUND 3
A. CHARACTERISTICS OF THE MABL 4
B. TECHNIQUE ASSUMPTIONS 5
1. The MABL is Well-Mixed 5
2. Optical Depth Within the MABL 6
3. Total Water Vapor Within the MABL 9
C. THE TECHNIQUE 11
1. Relative Humidity Parameterization 12
2. Integrated Properties and Model Outputs 12
3. Alternative Method of Computing RH(0) and ΔZ 14
4. The Iterative Process 16
5. Comparison of Constant and Changing Relative Humidity Lapse Rate 16
D. MEASUREMENT TECHNIQUES 18
1. Sea-Surface Temperature 19
2. Total Water Vapor 19
3. Optical Depth 21
E. SENSITIVITY OF THE TECHNIQUE TO MEASUREMENT ERROR . 22

III. VERIFICATION OF THE TECHNIQUE 27
A. VERIFICATION METHODS 27
1. Satellite Data Processing 27
2. Spatial and Temporal Differences in Technique Verification 28
B. CASE 1; OCTOBER, 1982 28
1. Synoptic Situation 28
2. Total Water Vapor and Optical Depth Verification 28
3. Technique Verification and Discussion 32
C. CASE 2; JULY, 1987 33
1. Synoptic Situation 33
2. SST and Total Water Vapor Verification 34

3. Technique Verification and Discussion 36
D. COMPOSITE VERIFICATION RESULTS 38
1. Total Water Vapor Comparison 38
2. Composite Scattergrams 38

IV. SURFACE RELATIVE HUMIDITY AND BOUNDARY LAYER HEIGHT IMAGES 41
A. SEQUENCE OF EVENTS TO PRODUCE AN IMAGE 41
B. OCTOBER 1982 IMAGES 43
C. IMAGES FROM JULY 1987 CASES 54
D. FASINEX IMAGES OF 23 FEBRUARY 1986 59

V. CONCLUSIONS AND RECOMMENDATIONS 65

REFERENCES 68

INITIAL DISTRIBUTION LIST 70

LIST OF TABLES

1. EFFECT OF VARIATIONS IN INPUT PARAMETERS ON RESULTS 17
2. TECHNIQUE INPUTS 18
3. EFFECT OF CHANGING C ON TECHNIQUE OUTPUTS AND % CHANGE FROM CONSTANT C METHOD 20
4. RH(0) AND MABL DEPTH VALUES AND T-TEST RESULTS FROM ERROR SENSITIVITY ANALYSIS 24
5. GROUND TRUTH COMPARISON FOR CASE 1: OCTOBER, 1982 32
6. TECHNIQUE COMPARISON FOR CASE 1 33
7. GROUND TRUTH COMPARISON FOR CASE 2: JULY, 1987 36
8. TECHNIQUE COMPARISON FOR CASE 2 39
9. EFFECT OF ERRORS IN TOTAL WATER VAPOR ON OUTPUT VALUES 40

LIST OF FIGURES

Fig. 1. Typical Marine Atmospheric Boundary Layer 4
Fig. 2. Saturation vapor density as a function of temperature: Bolton (1980) 6
Fig. 3. Value of extinction versus relative humidity from Durkee (1984) 8
Fig. 4. Profiles of extinction, potential temperature and relative humidity 10
Fig. 5. An example of a typical temperature and relative humidity profile 11
Fig. 6. Assumed relative humidity profile when layer relative humidity exceeds 97%. 15
Fig. 7. AVHRR spectral response functions from Lauritson et. al. (1979). 20
Fig. 8. Surface relative humidity histograms 23
Fig. 9. Boundary layer depth histograms 24
Fig. 10. Satellite subscene region for Case 1 - October, 1982 29
Fig. 11. Relative humidity and θ profile: 5 October 1982 30
Fig. 12. Synoptic Weather Pattern for Case 2 - 7 July, 1987 34
Fig. 13. Scattergrams For RH(0) and Z 40
Fig. 14. Sequence of Events to Produce an Image 42
Fig. 15. Visible image for 6 October 1982 44
Fig. 16. Sea-surface temperature image for 6 October 1982 46
Fig. 17. Total water vapor image for 6 October 1982 47
Fig. 18. Optical depth image for 6 October 1982 48
Fig. 19. Surface relative humidity image for 6 October 1982 49
Fig. 20. Boundary layer depth image for 6 October 1982 51
Fig. 21. Surface relative humidity image from 4 October 1982 52
Fig. 22. Boundary layer depth image from 4 October 1982 53
Fig. 23. Surface relative humidity image from 5 October 1982 55
Fig. 24. Boundary layer depth image from 5 October 1982 56
Fig. 25. Surface relative humidity image from 7 July 1987 57
Fig. 26. Boundary layer depth image from 7 July 1987 58
Fig. 27. Surface relative humidity image from 12 July 1987 60
Fig. 28. Boundary layer depth image from 12 July 1987 61
Fig. 29. FASINEX region and synoptic condition for 23 February 1986. 62

Fig. 30. Surface relative humidity image from 23 February 1986. 63
Fig. 31. Boundary layer depth image from 23 February 1986. 64

ACKNOWLEDGEMENTS

I wish to express my gratitude to several people without whose help this thesis would not have been possible. First, my wife Deborah gave me a tremendous amount of encouragement and moral support throughout the entire project. Professor Philip Durkee was equally instrumental in providing the necessary direction and professional expertise to guide the progress of the thesis from theory to actual satellite imagery. Professor William Shaw provided additional criticism to the final product. Finally, the technicians in the Interactive Digital Environmental Analysis (IDEA) lab, where all the images were produced, were especially helpful in all phases of the thesis. Specifically, Doug Burks, Jim Cowie, Rick Kohrs and Russ Schwanz provided the necessary expertise in all phases of image production from software programming to photographic production. A special note of thanks goes to Craig Motell who spent several extra hours debugging the programs that implemented the imaging technique.

I. INTRODUCTION

The marine atmospheric boundary layer (MABL) is a highly complex region of the environment that acts as the transition zone between the ocean and the free atmosphere. The unstable MABL is composed of a thin surface layer where turbulent fluxes are essentially constant with height, a well mixed region characterized by little vertical change of potential temperature or specific humidity and an inversion layer marked by large gradients in potential temperature, specific humidity and entrainment.

The ability to accurately describe and predict near surface conditions on a real time basis is crucial to the proper utilization of military weapons and sensors. Knowledge of the horizontal distribution of surface relative humidity and boundary layer depth could, for example, aid the intelligence staff of a battle group planning an air strike over hostile territory. Current vertical rawinsonde soundings provide no information about boundary layer characteristics except at the point of the rawinsonde launch. Mapping of the surface relative humidity and boundary layer depth fields on a regional scale can aid the meteorologist in predicting the refractive conditions for electromagnetic propagation that directly affect radar and weapons systems.

Currently, the marine boundary layer is observed through conventional methods such as rawinsonde and lidar soundings. However, they are severely limited in spatial extent and therefore do not provide a complete view of the spatial structure of the near surface environment. Mapping of boundary layer height and surface relative humidity on a large scale would greatly enhance our ability to effectively predict the physical processes that occur there. Variations in the layer structure with respect to the synoptic-scale environment could be studied in greater detail. The effect of diurnal variations on the MABL can also be observed in a new way. Finally, boundary layer mapping could provide data for numerical weather prediction with coverage that currently does not exist.

With the advent of meteorological satellites, large scale maps of specific meteorological phenomena have been produced that greatly enhance our knowledge of the air-sea interface. Sea-surface temperature, cloud cover and atmospheric aerosol content are examples of a few of the more commonly used products of satellite imaging. However, boundary layer measurements are extremely difficult to produce from satellite sounding techniques because of the poor vertical resolution associated with the current

satellite sounders. By utilizing multispectral techniques and making certain assumptions about the distribution of moisture, temperature and optical depth, the inherent errors associated with the satellite sounding method can be minimized. Kren (1987) has presented a method of obtaining boundary layer depth and relative humidity structure using multispectral measurements of sea-surface temperature, total water vapor and optical depth. The method has been tested with a model atmosphere under simulated conditions, and estimations of the boundary layer depth and surface relative humidity were within 5% of the actual values with zero measurement error. These results verify the validity of the assumptions made in producing the technique. The purpose of this thesis is twofold:

1. Test the validity of the technique under different synoptic conditions using rawinsonde data as verification of satellite measurements. Further, identify the limitations of the method as a result of cloud cover and inconsistent measurements.
2. Present a technique for mapping the surface relative humidity and boundary layer depth fields from data supplied by the Advanced Very High Resolution Radiometer (AVHRR) sensor.

In Chapter II, the technique is discussed in detail along with assumptions, measurement methods and statistical analysis of the cumulative effect of measurement errors. Chapter III describes the verification process with satellite data and Chapter IV presents results of case studies with images of boundary layer height and surface relative humidity provided. The final chapter consists of conclusions of this thesis with recommendations for future work.

II. THEORETICAL BACKGROUND

Kren (1987) proposed that the height of the MABL and parameterization of the relative humidity profile may be indirectly determined by satellite. The technique developed by Kren utilizes the AVHRR sensor to extract values of sea-surface temperature (SST), optical depth (τ) and total water vapor content (W). By making assumptions about the vertical structure of the MABL, the satellite derived estimations of SST, W and τ coupled with an estimate of atmospheric pressure at the sea surface can be employed in an iterative process to estimate boundary layer height and surface relative humidity. The characteristics of the MABL and the relationships between relative humidity, sea-surface temperature, optical depth and total water vapor will be reviewed in this chapter to form the basis of the technique. The assumptions and measurement procedures employed will also be discussed. Finally, a statistical analysis of the cumulative effect of satellite sensor measurement errors is examined.

The typical MABL can be separated into three horizontal layers as shown in Fig. 1. The surface layer is confined to the first tens of meters above the sea surface. Here strong gradients of wind, temperature and moisture generate fluxes of heat and moisture. It is important to realize that no turbulent transport takes place across the air-sea interface (Businger, 1985). The ocean surface acts as a barrier to the exchange of temperature and moisture. The major transport of the mixed layer quantities is through horizontal advection in the surface layer. The stability of the layer is dependent on the air-sea temperature difference. An unstable condition generally exists when the air is cooler than the water and turbulent convection occurs. The stronger the convection, the thinner the surface layer. Above this and extending to the base of the inversion layer is the mixed layer, characterized by turbulent eddies which mix potential temperature and specific humidity to constant values throughout its vertical extent. The thin inversion layer, also on the order of tens of meters, is where turbulence is extinguished by stable stratification and where strong vertical gradients of potential temperature and specific humidity exist.

The balance of processes that act to determine the structure of the MABL can be summarized as follows:

1. Fluxes of heat and moisture enter the base of the MABL in the surface layer.

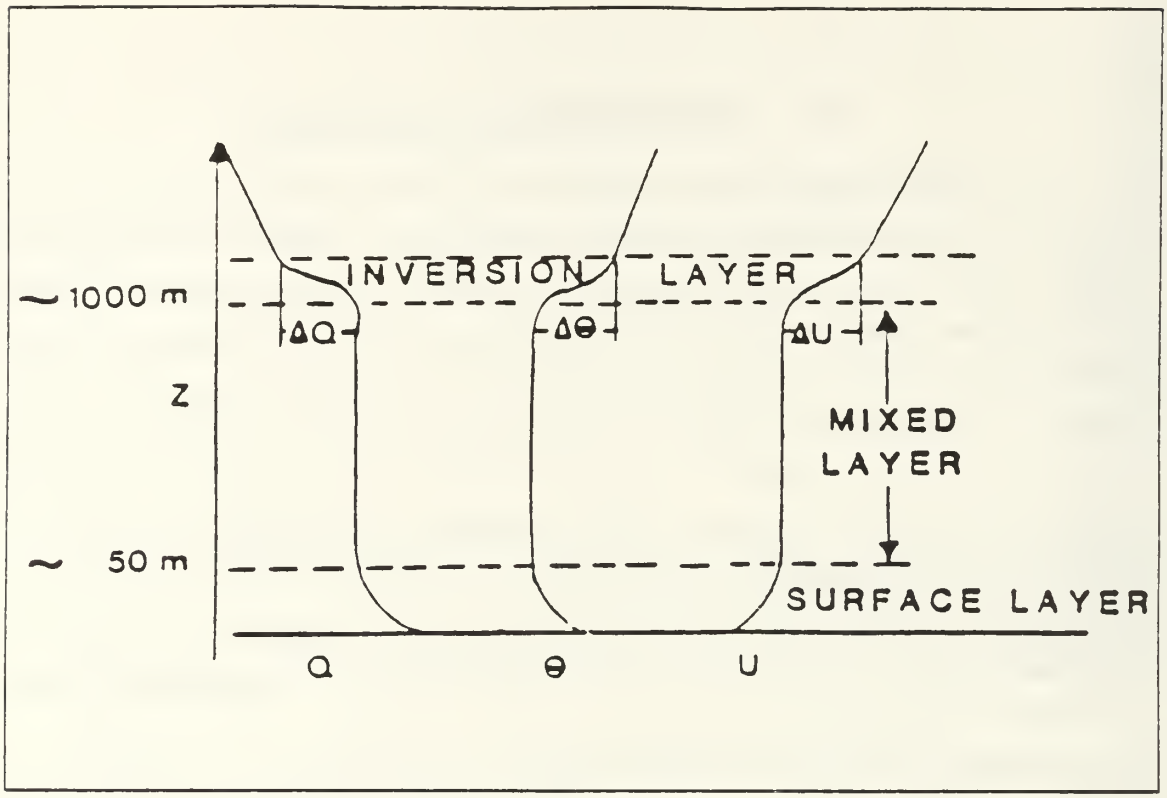

Fig. 1. Typical Marine Atmospheric Boundary Layer

2. Heat and moisture are transferred upward in the boundary layer by turbulent eddies which also entrain dry free atmospheric air through the inversion layer. This acts to deepen the MABL.

3. Subsidence from above forces the layer down toward the surface and intensifies the inversion layer.

A. CHARACTERISTICS OF THE MABL

Within the well mixed MABL, potential temperature, specific humidity and mixing ratio tend to be constant with height. Adiabatic mixing, described in Rogers (1979), is the process whereby samples of air from different pressure levels are brought adiabatically (without gain or loss of heat) to the same pressure level and mixed. This is an ongoing process within the well-mixed layer and is responsible for maintaining the constant profiles of specific humidity and mixing ratio.

The technique for estimating boundary layer depth and surface relative humidity developed here takes advantage of these simple distributions and is based on the relationships of temperature and relative humidity. Relative humidity depends on the vapor density and the saturation vapor density of ambient air within the boundary layer:

$$RH = \frac{\rho_w}{\rho_{ws}} \times 100\%. \quad (1)$$

While vapor density reflects the amount of water vapor present and has no temperature dependence, saturation vapor density is directly related to temperature via the Clausius-Clapeyron equation. Bolton (1980) developed a formulation for saturation vapor density as a function of temperature which yields errors of less than 0.1% for temperatures greater than 0 °C.

Fig. 2 shows a plot of saturation vapor density as a function of temperature. Since relative humidity is inversely proportional to saturation vapor density and temperature decreases with height in a well-mixed boundary layer, relative humidity increases with increasing height.

B. TECHNIQUE ASSUMPTIONS

The technique developed by Kren is based on three fundamental assumptions about the MABL:

1. The MABL values of potential temperature and specific humidity are well mixed.
2. Aerosol optical depth at red-visible and near infrared wavelengths results from particles that are confined primarily within the MABL.
3. The total atmospheric water vapor content is confined primarily within the MABL.

The validity of each of these assumptions will be discussed briefly to identify the conditions under which the technique can be applied.

1. The MABL is Well-Mixed

Turbulent mixing within the layer is the process that produces homogeneous potential temperature and water vapor mixing ratio regimes. This mixing occurs because of buoyancy and shear effects. Strong buoyancy production and turbulent kinetic energy within the MABL is usually suppressed because of the inability of the sea surface to warm sufficiently during daylight hours. At night,the heat capacity of the ocean prevents radiative cooling of the surface from causing the formation of a stable layer. Therefore, buoyancy effects are small, and the MABL remains near neutral with only slight diurnal variations.

Wind shear in the surface layer results in shear production of turbulent kinetic energy which also mixes the MABL. Overall, the combination of buoyancy production and shear production results in a fairly well-mixed boundary layer. While this holds true for a significant portion of the global air-sea interface, there are regions where the

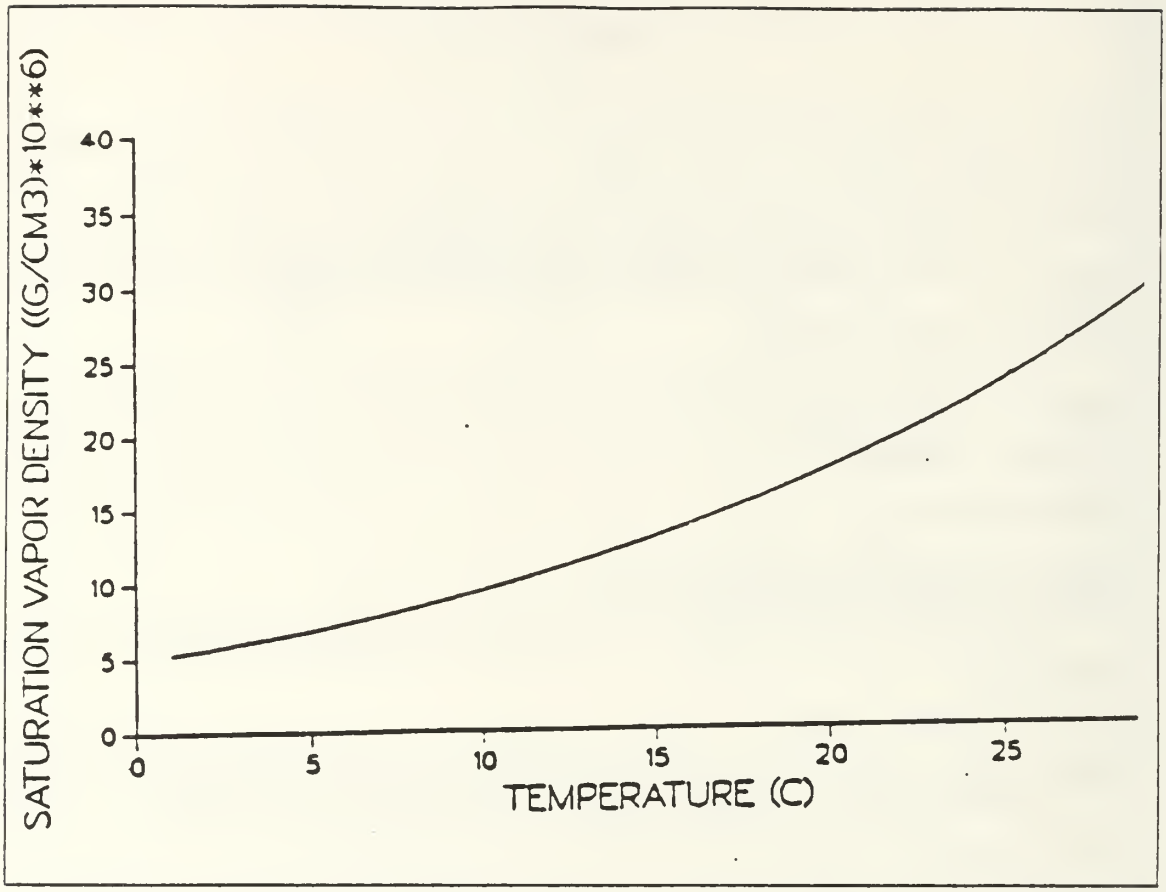

Fig. 2. Saturation vapor density as a function of temperature: Bolton (1980)

combination of environmental factors leads to a highly stable MABL in which mixing is suppressed. One example is on the west coast of continents under a very strong subsidence inversion. Cold sea temperatures due to upwelling, coupled with low wind shear can produce vertical distributions of state variables that deviate from the assumptions presented. The farther the deviation from the assumptions, the greater the error in the estimates of surface relative humidity and boundary layer height. This relationship will be shown in the next chapter.

2. Optical Depth Within the MABL

It is important to first review the radiometric quantities which affect optical depth. The extinction coefficient, β is a measure of the probability of a photon being scattered or absorbed. The extinction coefficient has two components, extinction due to scattering (β_{scat}) and to absorption (β_{abs}). Shettle and Fenn (1979) describe atmosphere

aerosol distributions, and for marine particles they conclude absorption is small and the scattering coefficient is equivalent to the extinction coefficient. This approximation is used here. The extinction coefficient is defined as:

$$\beta_{ext} = \int_0^\infty \pi r^2 Q_{ext}(m,r) \frac{dN(r)}{dr} dr, \tag{2}$$

where πr^2 is the cross sectional area for a given particle radius, Q_{ext} is extinction efficiency (dependent on the complex refraction index (m) and particle radius (r)), and dN(r) dr describes the distribution of particles by radius. Variations in each of these three factors produce corresponding changes in extinction. Kren, (1987) gives a detailed analysis of the effects of each of the three factors. Summarizing, Fitzgerald (1979) shows that the dominant term affecting extinction is particle size. Durkee (1984) found a relationship between extinction and relative humidity consistent with Fitzgerald's work. The functional relationship:

$$\beta = \frac{1}{A(B - RH)}, \tag{3}$$

where A = .2998, B = 99.8999 and RH = relative humidity is graphically illustrated in Fig. 3. The relationship is based on aircraft measurements of extinction within the MABL off the southern California coast, 1982.

Atmospheric optical depth is defined as the vertical integral of the extinction coefficient ($\beta_{ext.}$) through the depth of the atmospheric column (dz):

$$\tau = \int_0^{\Delta z} \beta_{ext} dz. \tag{4}$$

Since β_{ext} has units of km^{-1} and is integrated over dz, optical depth is a dimensionless quantity that describes the amount of attenuation within the atmosphere. Typical values range from .01 to over 1.0 for high aerosol content conditions.

Scattering of solar radiation toward a satellite sensor is due to a combination of molecular and particle scattering. Rayleigh scattering of molecular constituents within the atmosphere is nearly constant away from strong gradients of temperature and pressure, as in the MABL. Mie scattering occurs primarily because of interactions with marine particles within the MABL. A second contribution due to Mie scattering comes from aerosols above the boundary layer advected over water by continental sources. A

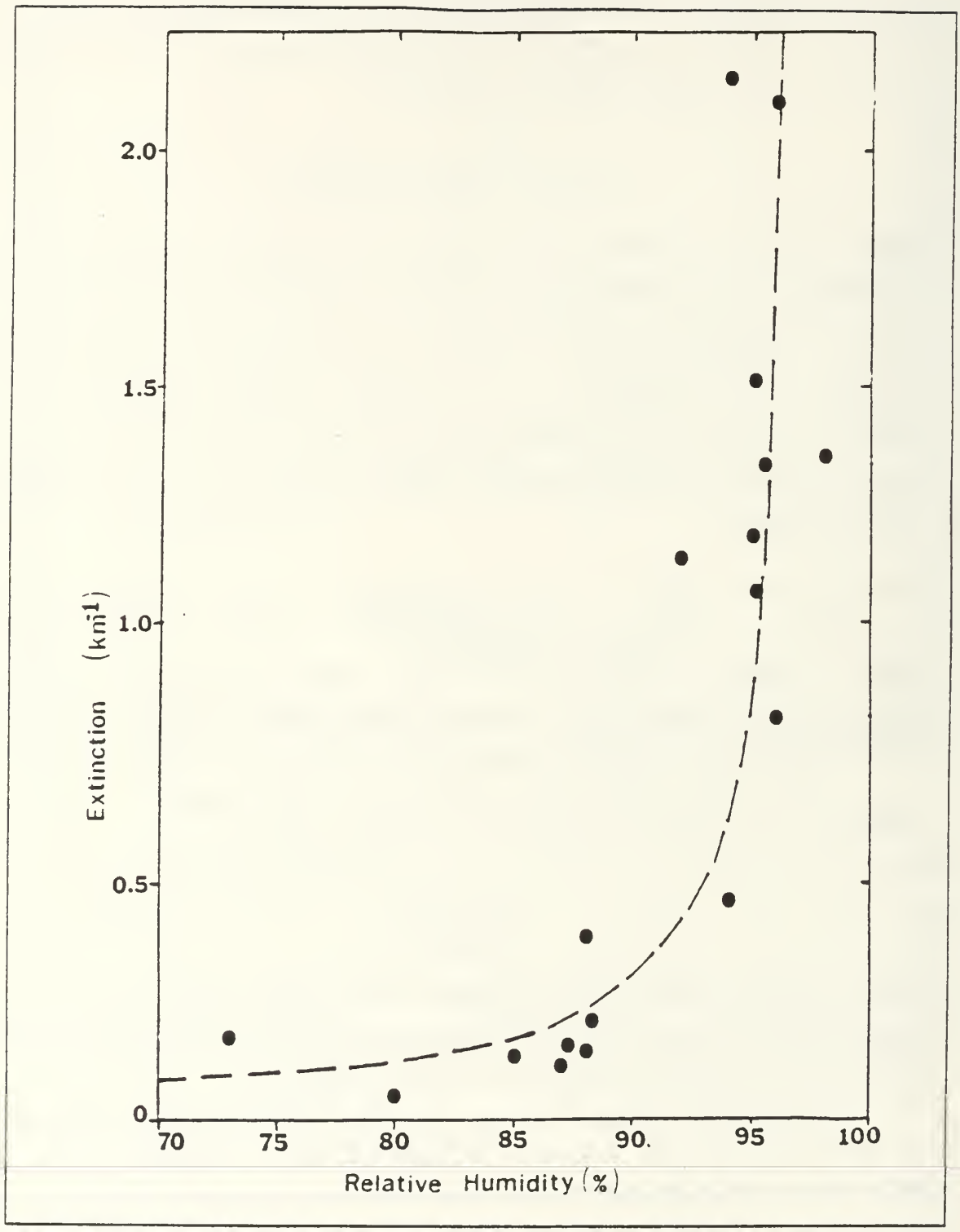

Fig. 3. Value of extinction versus relative humidity from Durkee (1984)

third source of upwelled radiance is reflection from the ocean surface and from windblown whitecaps. Koepke and Quenzel (1981) shows that ocean surface contributions to reflected solar radiance are minimized at wavelengths used to measure optical depth on the AVHRR, in this case, channel 1 (0.63 μm).

As shown in this section, optical depth is a parameter that embodies a variety of physical processes. By limiting the technique to well-mixed regions and by using channel 1 of the AVHRR, the assumption of optical depth being confined to the MABL can be supported. Fig. 4 shows the profiles of extinction, relative humidity and potential temperature for 5 October 1982 off the coast of California (Durkee, 1984). As can be seen from the extinction profile, the majority of optical depth is confined to the boundary layer.

3. Total Water Vapor Within the MABL

The total water vapor content (W) in a column of atmosphere is defined as the vertical integration of the vapor density, ρ_w, within the column. Under the assumption that the total water vapor is confined to the MABL, the vapor density must also be confined to the MABL and the integration distance (Δz) becomes the depth of the boundary layer:

$$W = \int_0^{\Delta z} \rho_w dz. \tag{5}$$

Nieman (1977) discusses maritime air masses associated with a strongly subsiding troposphere. Over oceanic regions, the lower troposphere is moistened by fluxes across the air-sea interface, resulting in a moist MABL beneath a dry, free troposphere. This is illustrated in Fig. 4 with the relative humidity profile from an actual case study and in Fig. 5 in schematic form where profiles of relative humidity and temperature are displayed. The water vapor content above the subsidence inversion is minimized and the assumption of total water vapor being confined to the MABL holds under these conditions.

The assumptions required for the technique to function properly constrain its applicability. The procedures for extracting sea-surface temperature, optical depth and total water vapor from satellite detected radiance require a cloud free atmosphere. The technique can be applied within well-mixed MABL's, away from continental aerosol above the boundary layer so optical depth above the layer is minimized and in regions of subtropical high pressure anticyclones where water vapor is minimized above the

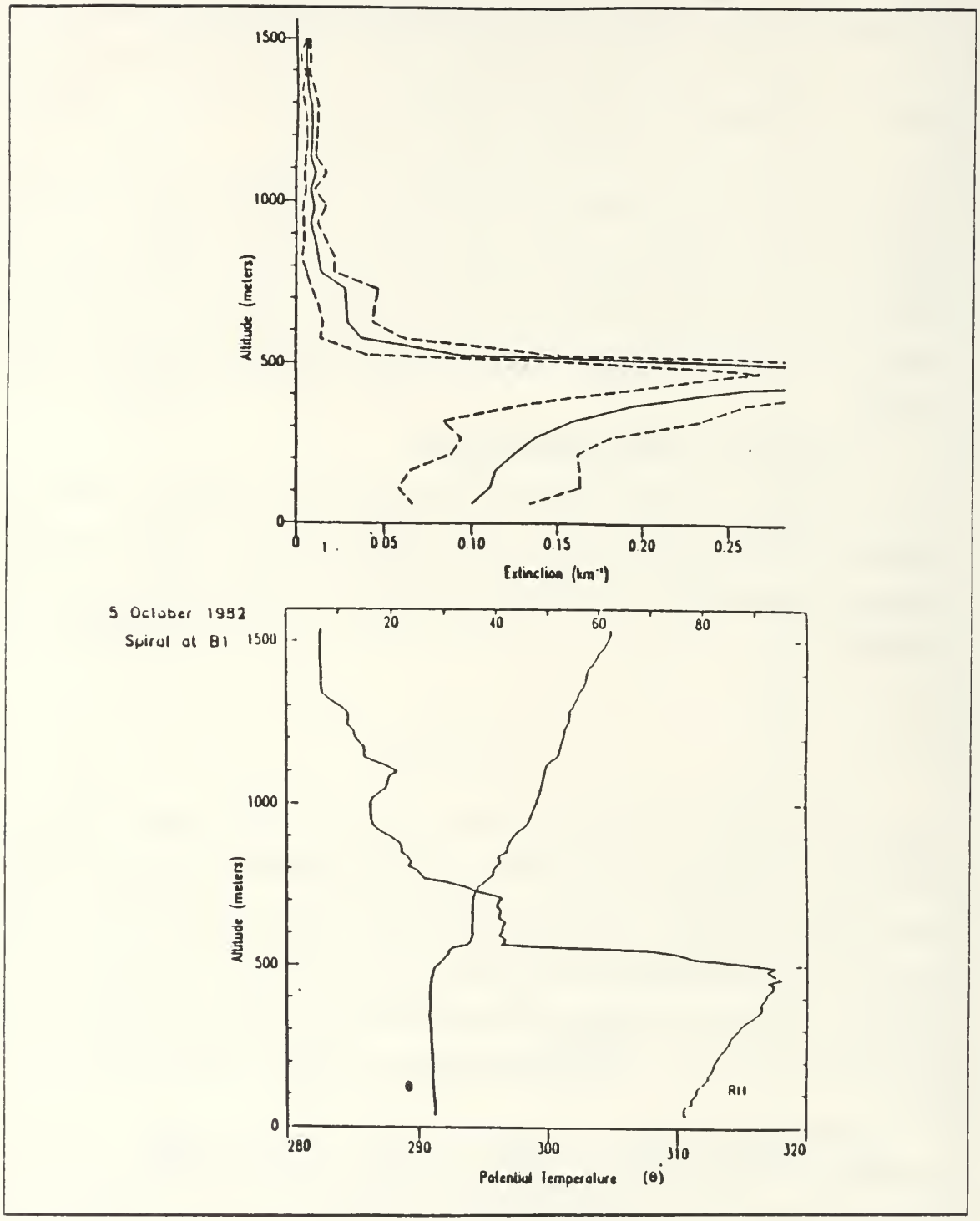

Fig. 4. Profiles of extinction, potential temperature and relative humidity: Case B1 from Durkee (1984).

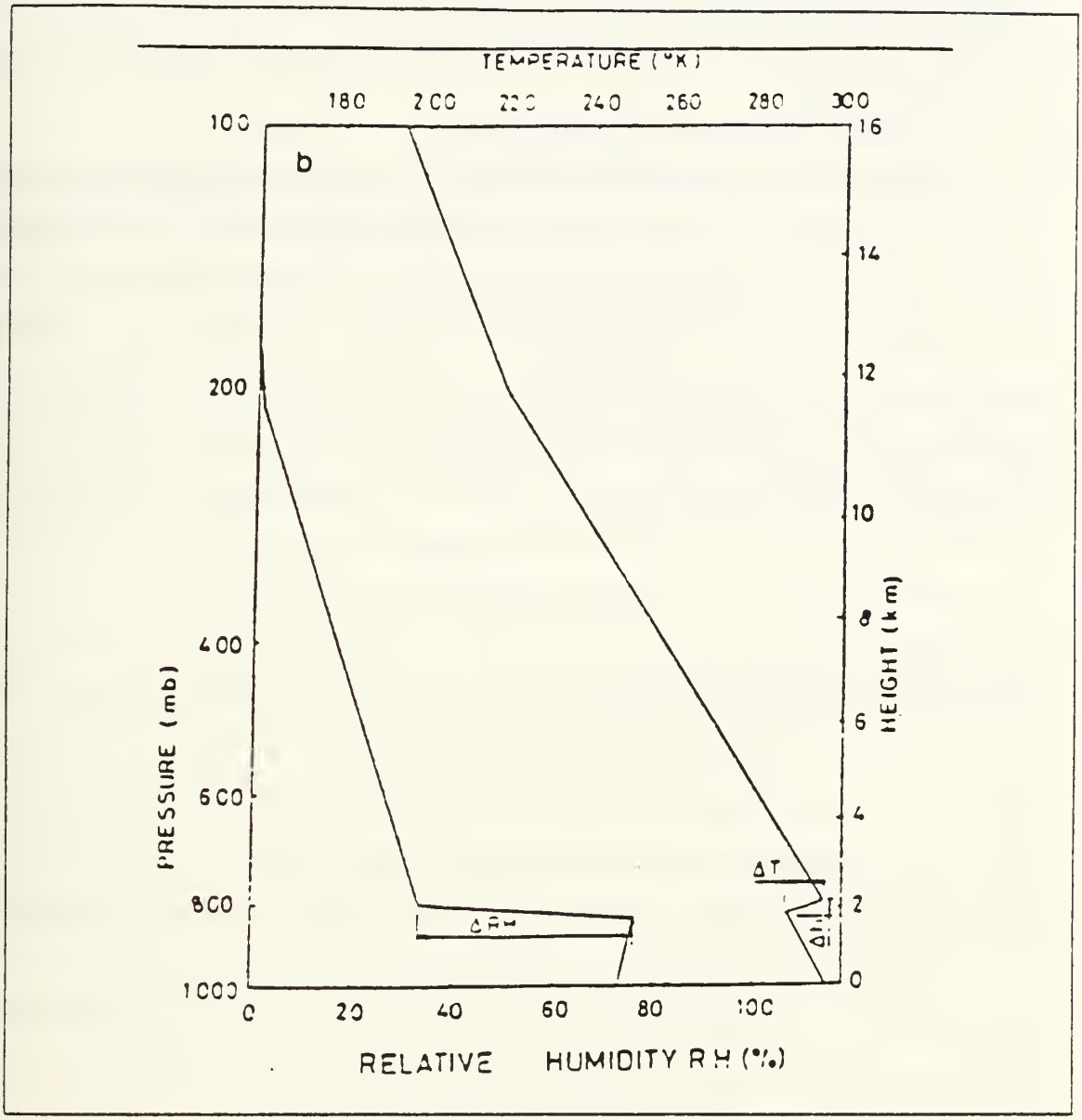

Fig. 5. An example of a typical temperature and relative humidity profile: After Nieman (1977)

MABL. Errors in the estimation of surface relative humidity and boundary layer depth increase as deviations from the initial assumptions increase..

C. THE TECHNIQUE

The assumptions described in the previous section of optical depth and total water vapor confined within the MABL enable Eqs. 4 and 5 to be combined through the

common vertical integration distance (Δz). The combined equations can be solved for surface relative humidity by substituting for the extinction and vapor density in terms of relative humidity.

1. Relative Humidity Parameterization

Kren (1987) developed relative humidity profiles for technique validation from a model atmosphere. For shallow layers, the typical relative humidity profile increases linearly with height. As the layer becomes deeper, the linear parameterization breaks down. This deviation is explained using Eq. 1 and Fig. 2. In deeper layers, because of the dry adiabatic lapse rate, the change in temperature through the depth of the layer allows the nonlinearity of the saturation vapor density function to influence the relative humidity profile. For thin layers (< 1 km), the non-linearity of the vapor density function is small and the relative humidity profile can be approximated by a straight line. The parameterization is a linear function with height:

$$RH(z) = RH(0) + Cz, \tag{6}$$

where RH(z) is the relative humidity at any height z, RH(0) is the surface value and C describes the percentage increase in relative humidity from the surface value to the top of the layer when normalized to 1 km. Surface relative humidity is defined as the extrapolation of the linear relative humidity profile down to zero meters. Theoretically, the surface relative humidity over the ocean surface is always 100%, however for the purposes of the parameterization of the relative humidity lapse rate, the above definition of the extrapolated value is used.

The factor C, analogous to a relative humidity lapse rate, was found in the technique to be variable with boundary layer depth, sea-surface temperature and surface relative humidity. Kren (1987) examined variations in boundary layer depth and found a functional relationship:

$$C = 14.07 + 3.3333(\Delta z), \tag{7}$$

where Δz is the layer thickness in km and C is in dimensions of %/km. The effect of sea-surface temperature and surface relative humidity on the lapse rate will be discussed in the next section.

2. Integrated Properties and Model Outputs

By substituting Eq. 3 for extinction as a function of relative humidity, optical depth can be solved for analytically:

$$\tau = \frac{1}{A}(B - RH(z))\Big]_0^{\Delta z}, \tag{8}$$

where A and B are defined above, RH(Δz) is the relative humidity at the top of the MABL and RH(0) is the surface relative humidity. If extinction is again integrated with relative humidity parameterized by Eq. 6, the result is:

$$\tau = -\frac{1}{AC}\ln\frac{AB - ARH(0) - AC\Delta z}{AB - ARH(0)}. \tag{9}$$

Simple layer averaging of extinction would tend to underestimate the value of optical depth because of the nonlinear relationship between relative humidity and extinction at higher relative humidities, (Fig. 3). Therefore, it is necessary to seek an analytical solution (Eq. 9) for the integration of extinction.

Total water is the vertical integration of vapor density through the height of the atmospheric column. By choosing a constant mean layer vapor density and extending the integration through the depth of the MABL, the equation can be solved such that:

$$W = \frac{(RH(\Delta z)/2)\rho_{ws}(T(\Delta z/2))}{100}, \tag{10}$$

where $\rho_{ws}(T(\Delta z/2))$ = the saturation vapor density based on the layer temperature at height $\Delta z/2$. Assuming that the value of vapor density at $\Delta z/2$ is representative for the MABL, total integrated water vapor can be solved for in terms of relative humidity and saturation vapor density through substitution of Eq. 1:

$$W = \frac{(RH(0) + C\Delta z/2)\rho_{ws}(T(\Delta z/2))}{100}\Delta z. \tag{11}$$

Eqs. 9 and 11 can be manipulated to solve for the layer depth (Δz):

$$\Delta z = \frac{AB - (AB - ARH(0))\exp(-\tau AC) - ARH(0)}{AC}, \tag{12}$$

and

$$\Delta z = -\frac{RH(0) \pm \sqrt{RH(0)^2 + 200CW\rho_{ws}(T_{lyr})}}{C}. \tag{13}$$

In Eq. 13, the positive root of the radical in the quadratic is always selected. Through the common factor Δz, Eqs. 12 and 13 can be combined which leads to a solution for surface relative humidity (RH(0)):

$$[1-(e^{-\tau AC})^2]\times RH(0)^2$$

$$+[2Be^{-\tau AC}(e^{-\tau AC}-1)]\times RH(0)$$

$$-B^2(1-e^{-\tau AC})^2+2.0\times 10^{-3}CW/\rho_{ws}(T_{lyr})=0. \tag{14}$$

Solution of this quadratic formula yields the surface relative humidity value which is substituted into Eq. 12 for determination of MABL thickness.

The technique will fail if measurements of optical depth, total water vapor and sea-surface temperature are inconsistent. Solutions to Eq. 14 produce two complex numbers. Any time the imaginary part is non-zero, the solution for surface relative humidity is indeterminate. The technique incorporates this test to ensure that only purely real solutions are used.

3. Alternative Method of Computing RH(0) and ΔZ

Because it is assumed that the relative humidity increases with height within the boundary layer, it is possible to have cases where saturation is reached. If this happens, the relationship between the input variables of sea-surface temperature, total water vapor and optical depth is changed and a new set of equations must be employed to balance the equations. Fig. 6 shows the assumed relative humidity profile when the parameter C allows for the relative humidity within the layer to exceed 97%. Since cloud free conditions is an initial assumption, it is necessary to cap the profile prior to saturation and as an approximation to this case, the relative humidity is held constant at 97% to the top of the layer.

The alternative set of equations is derived by substituting 97% for RH(z) in Eqs. 8 and 10 and solving each of these for Δz:

$$\Delta z=\frac{[(B-97)\times[\tau AC+\ln(B-97)/(B-RH(0))]+(97-RH(0))]}{C} \tag{15}$$

$$\Delta z=-\frac{(97)^2-(RH(0))^2}{194\times C}+\frac{100\times W}{97\times\rho_{ws}}+\frac{97-RH(0)}{C}. \tag{16}$$

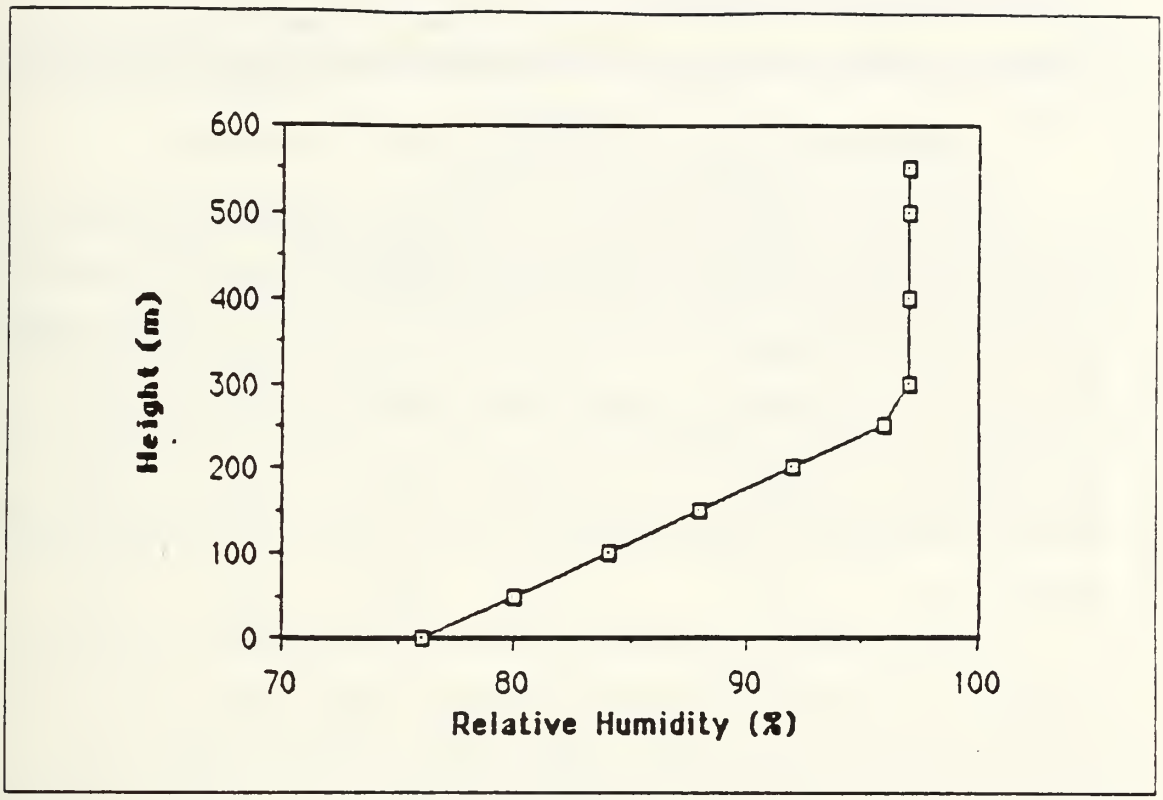

Fig. 6. Assumed relative humidity profile when layer relative humidity exceeds 97%.

By equating the two equations, a transcendental equation is produced:

$$\frac{[(B-97)\times[\tau AC+\ln(B-97)/(B-RH(0))]+(97-RH(0))]}{C}$$

$$+\frac{(97)^2-(RH(0))^2}{194\times C}-\frac{100\times W}{97\times\rho_{ws}}-\frac{97-RH(0)}{C}=0. \qquad (17)$$

The roots of the equation are determined numerically. Once surface relative humidity is determined, it can be substituted into Eq. 15 to find boundary layer thickness.

Initially, surface relative humidity and boundary layer thickness are estimated using Eqs. 12 and 14. Using the relative humidity lapse rate, C, the proper relative humidity profile is then determined after each iteration. If 97% relative humidity is reached within the layer, the technique uses Eqs. 15 and 17 for further refinement of the surface

relative humidity and boundary layer depth estimations. If saturation is not reached, the technique uses Eqs. 12 and 13 to estimate surface relative humidity and boundary layer depth.

4. The Iterative Process

Provided the input measurements of sea surface temperature, optical depth and total water vapor are reasonably consistent, the technique iterates on Eqs. 12 and 14 and converges to a boundary layer depth and surface relative humidity. Iteration is required because of the lack of information initially about the MABL. Mid-layer temperature and layer depth are unknown at the onset. Layer depth and mid-layer temperature can be estimated after a calculation of the surface relative humidity is made. With these variables defined, recalculated values of the parameter C and the layer saturation vapor density are determined. Iteration is necessary since ρ_{w_s} and C are factors in the quadratic equation.

The determination of the initial value of C was described at the beginning of this section. The initial value of the layer saturation vapor density is found from the sea-surface temperature. Succesive iterated values are the mid-layer values as the hypsometric formula and Poisson's equation are applied to the computed layer thickness and temperature respectively. A detailed treatment of this process can be found in Kren (1987).

5. Comparison of Constant and Changing Relative Humidity Lapse Rate

Kren (1987) investigated the dependence of the parameter C to boundary layer depth. He produced sensitivity studies that quantified the response of the method as a function of the perturbation of sea surface temperature, total water vapor and optical depth. Standard deviations based on reasonable measurement errors were used for each of the variables of sea-surface temperature, total water vapor and optical depth to determine the high and low values of each output; 10% for optical depth, 1.0 °C for SST and 0.10 g/cm^2 for total water vapor. The results for simulated boundary layer depths of 500, 1000 and 1500 m are presented in Table 1. Upon further investigation it was found that variations in SST and surface relative humidity also affect the value of C. To assess the effect of the deviations in these variables, outputs of surface relative humidity and boundary layer depth were generated under model atmosphere conditions for the combinations of inputs listed in Table 2. These values represent the range of each of the parameters in regions of the world where the technique is most applicable. A linear interpolation scheme was developed which produces a value of C, the relative humidity

TABLE 1
EFFECT OF VARIATIONS IN INPUT PARAMETERS
ON RESULTS

	Layer Depth (m)				RH(0) %		
	500	1000	1500		500	1000	1500
SST (°C)							
+ 1.0	457.6	907.1	1337.5		72.6	73.0	73.9
-1.0	557.7	1101.2	1632.2		66.5	66.8	66.7
TAU							
+ 10%	478.3	962.0	1459.0		73.5	72.9	71.3
-10%	544.1	1046.0	1485.2		64.1	66.4	69.9
W (G CM2)							
+ 1.0	635.1	1109.6	1582.1		61.7	66.6	68.1
-1.0	406.5	895.6	1361.3		75.7	73.3	73.1

lapse rate, for all the possible combinations of inputs. In this way, the technique accounts for changes in the slope of the relative humidity profile. Table 3 shows model results of surface relative humidity and boundary layer depth values comparing those generated with the above linear function lapse rate to those with the changing lapse rate. A positive value of $\Delta\%$ represents an improvement of the changing lapse rate process over the constant lapse rate process.

As can be seen from the table, there is little difference in the sensitivity of the parameters when the variable lapse rate is taken into account. However, there are some interesting patterns present. In most cases, the variable lapse rate method improves the technique on one side of the given output variable significantly more than it degrades the result on the other. As an example, in the sea-surface temperature cases for layer depth, the average improvement of the changing lapse rate method for a -1.0 °C error is 0.6% and the average degradation for a positive 1.0 °C is 0.17%. Differences of 0.17% for a 1000 m boundary layer depth correspond to an error of less than 2 m. Also, the differences between the two methods increase as the depth of boundary layer increases. This is a manifestation of the nonlinearity of the temperature dependence in deeper layer depths. Further, the changing lapse rate method is considerably slower because of the necessity to interpolate in a three dimensional matrix. The increase in computational time offsets the near negligible improvement in the changing lapse rate

TABLE 2
TECHNIQUE INPUTS FOR RELATIVE HUMIDITY LAPSE RATE COMPARISON

BOUNDARY LAYER DEPTH(m)	SST (°C)	SURFACE RELATIVE HUMIDITY (%)
200	12	60
400	14	65
600	16	70
800	18	75
1000	20	80
1200		
1400		
1600		

method over the constant lapse rate method. The combination of the small improvement in accuracy and slower computational time make the changing lapse rate method less attractive than the constant lapse rate method. One of the objectives of the technique to estimate surface relative humidity and boundary layer depth is to provide real time outputs and to this end, the constant lapse rate has been incorporated into the technique.

D. MEASUREMENT TECHNIQUES

As stated in the introduction, the technique is based on measurements derived from a single sensor, the Advanced Very High Resolution Radiometer (AVHRR). Fig. 7 shows the spectral response function for the AVHRR. Channel 1 (0.63 μm) is used in optical depth estimation and reflectance testing for cloud contamination, and channels 4 (10.5 μm) and 5 (12.0 μm) for sea-surface temperature and total water vapor estimations. The advantages of utilizing a single sensor such as the AVHRR to provide the necessary measurements of sea-surface temperature, optical depth and total water vapor are twofold. First, a single sensor alleviates the differences in resolution between multiple sensors. Where one sensor may have a resolution of 1 km, another may have a resolution of 25 km. Second, the time taken in processing data is less from a single sensor than from multiple sensor techniques. While there are documented methods of extracting these required parameters from other sensors on other satellites, the technique utilizing

TABLE 3
EFFECT OF CHANGING C ON TECHNIQUE OUTPUTS AND % CHANGE FROM CONSTANT C METHOD

	Layer Depth (m)			RH(0) [%]		
SST (°C)						
+ 1.0	455.6	906.5	1337.4	72.7	73.4	75.2
Δ%	-0.4	-0.1	0.0	-0.1	-0.5	1.0
-1.0	554.0	1099.9	1614.0	66.8	67.5	69.5
Δ%	0.8	0.3	0.8	0.4	1.0	4.0
τ						
+ 10%	476.7	961.3	1448.3	73.6	73.3	73.5
Δ%	-0.2	-0.1	-0.7	-0.1	-0.6	-1.5
-10%	539.4	1043.6	1484.5	64.7	67.1	71.4
Δ%	1.2	0.4	-0.1	0.7	1.0	-1.9
$W(Kg/m^2)$						
+ 1.0	628.6	1106.5	1568.5	62.3	67.4	70.6
Δ%	2.0	0.3	0.9	0.7	1.2	2.2
-1.0	405.1	895.2	1364.6	75.7	73.6	74.5
Δ%	-0.2	0.0	0.2	-0.1	-0.2	0.2

the AVHRR will be discussed here. Verification of the methods will be discussed in the next chapter.

1. Sea-Surface Temperature

Satellite multi-channel sea-surface temperature (MCSST) methods have existed since 1983 and are continually being refined. McClain (1985) presents a method currently used by NOAA that is applicable for the five-channel AVHRR sensors (NOAA-7 and NOAA-9). MCSST takes advantage of the differential water vapor absorption in the infra-red channels 4 and 5 by splitting the 10-13 μm absorption window. The 10 μm band is virtually clean with respect to water vapor while the 13 μm band is on the edge of the water vapor absorption window. By comparing the brightness temperatures of the two bands, the water vapor contamination can be accounted for and the true sea-surface temperature determined. The rms error from this method is less than 1.1 °C.

2. Total Water Vapor

Channels 4 and 5 are also utilized in extracting total water vapor from the atmosphere. Instead of correcting for water vapor absorption, the varying degrees of absorptance between channels 4 and 5 may be utilized to provide information about the

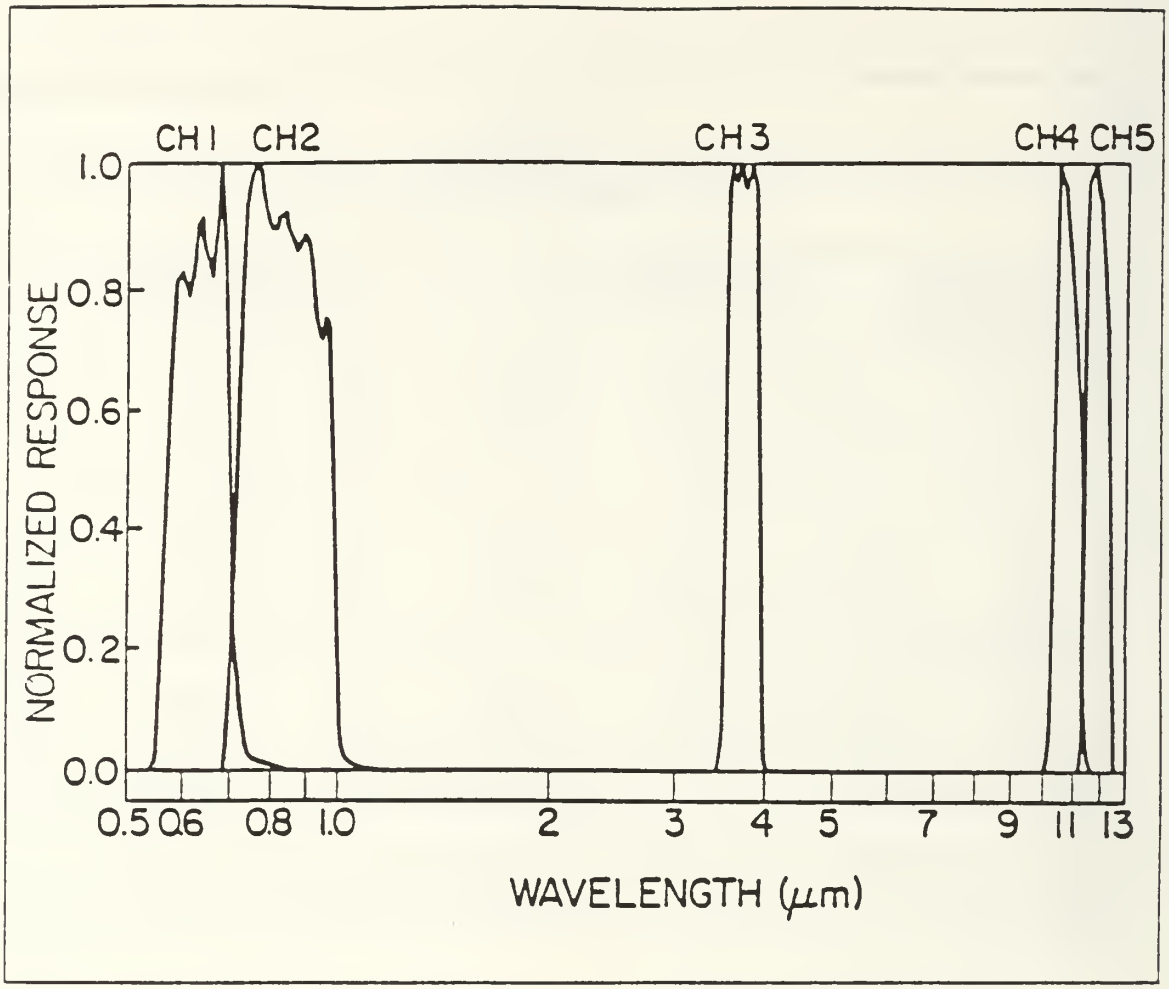

Fig. 7. AVHRR spectral response functions from Lauritson et. al. (1979).

amount of water vapor in the MABL. Dalu (1986) found the relationship between sea-surface temperature and total water vapor to be a function of the satellite zenith angle (θ):

$$W = A(T_4 - T_5)\cos\theta, \tag{18}$$

where $A = g(W)/(k(T_s - \overline{T}))$; g(W) is a function of water vapor, k is an absorption coefficient and $(T_s - \overline{T})$ is the difference between the sea-surface temperature and the mean radiative temperature of the atmosphere. Dalu analyzed a large range of atmospheric profiles of temperature and relative humidity and found A = 1.96 g/cm^2 to hold for typical atmospheric water vapor contents.

3. Optical Depth

Liou (1980) describes the theory behind radiative transfer to estimate optical depth. The amount of radiance reflected by the atmosphere measured at the satellite is directly proportional to the amount of optically active scatterers in the atmosphere.

The radiative transfer equation which describes the scattering of solar radiation in the atmosphere may be written from Liou (1980) as:

$$\mu \frac{dL(\tau, \Omega)}{d\tau} = L(\tau, \Omega)$$

$$- \frac{\omega_0}{4\pi} \int_{4\pi} L(\tau, \Omega') P(\Omega, \Omega') d\Omega'$$

$$- \frac{\omega_0}{4\pi} \pi F_0 P(\Omega, \Omega_0) \exp(-\tau/\mu), \tag{19}$$

where:

L	=	diffuse intensity or radiance,
τ	=	optical depth,
ω_0	=	single scatter albedo,
μ	=	cos θ (θ is the observation zenith angle),
Ω	=	solid angle (θ , ϕ) (ϕ = azimuth angle) and
P(Ω Ω')	=	inconing radiative flux.

By assuming the single scattering approximation and that upward intensities from the ocean surface and subsurface are negligible, the reflected intensity for a finite atmosphere with total optical depth (τ_1) is:

$$L(0; \mu, \phi) \sim \frac{\omega_0 F_0}{4\pi} P(\Theta) \tau_1, \tag{20}$$

from Durkee (1984). Therefore, reflected intensities are directly proportional to optical depth, scattering phase function, satellite viewing geometry and single scattering albedo. Channel 1 (0.63 μm) of the AVHRR sensor in conjunction with known values of the scattering phase function, single scattering albedo and satellite geometry then can be used to estimate optical depth.

E. SENSITIVITY OF THE TECHNIQUE TO MEASUREMENT ERROR

Errors exist in each of the methods to estimate sea-surface temperature, optical depth and total water vapor by the AVHRR because of the inability of a sensor to produce perfect measurements. A statistical analysis was performed based on simulated data and model boundary layer conditions in order to assess the cumulative effects of errors in the measurements of sea-surface temperature, total water vapor and optical depth. The two parameters most often used to describe a population are the mean and the standard deviation. The mean defines the most likely value of a distribution and the standard deviation defines the amount of spread within the population. Two types of analyses were conducted; a histogram study to graphically illustrate the spread of the population and a t-test to assess the range of the expected mean.

The analysis was performed with a 1000 m MABL depth, 70 and 80% surface relative humidity and 20 and 25 °C SST. The original sensitivity study conducted by Kren and the subsequent effect of changing the relative humidity lapse rate used errors of 1.0 °C, 0.10 gm/cm^2 and 10% for sea-surface temperature, total water vapor and optical depth respectively. After further literature review and actual satellite measurements, it has been determined that more realistic errors for the three variables are 1.0 °C, 0.20 gm/cm^2 and 20% for sea-surface temperature, total water vapor and optical depth respectively. The model was run with 30 random combinations of inputs within this broader range of errors.

To assess the effect of combinations of input errors on the expected spread of the outputs, histograms were produced that graphically display the standard deviation in each of the cases. Fig. 8 shows the surface relative humidity histograms while Fig. 9 shows the boundary layer depth histograms.

Standard deviations range from 2.1 to 6.3 in the surface relative humidity cases and from 94.9 to 168.6 in the boundary layer depth cases. The general trend in surface relative humidity cases is toward smaller standard deviation as the surface relative humidity increases. The same correlation holds true for the boundary layer depth cases. As shown in Fig. 3, relative humidity is effected by extinction and thus optical depth in a near exponential increase as relative humidity is increased. Even though the cases were run at 70% and 80% surface relative humidity where the sensitivity of relative humidity to extinction is not that significant, the layer relative humidity will approach higher values in the cases of higher surface relative humidity. Therefore the technique should prove more accurate in cases of higher surface relative humidity where the dependency

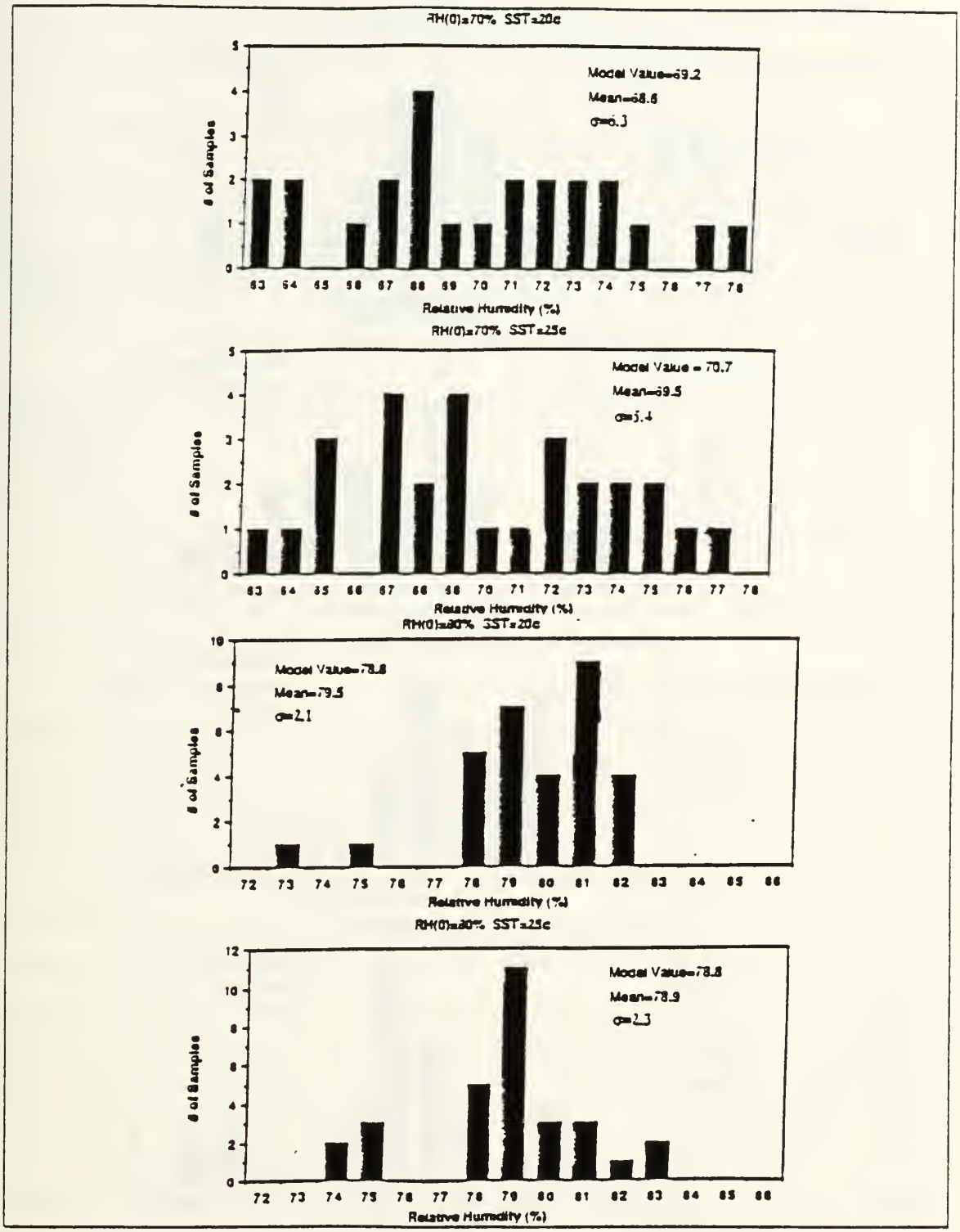

Fig. 8. Surface relative humidity histograms

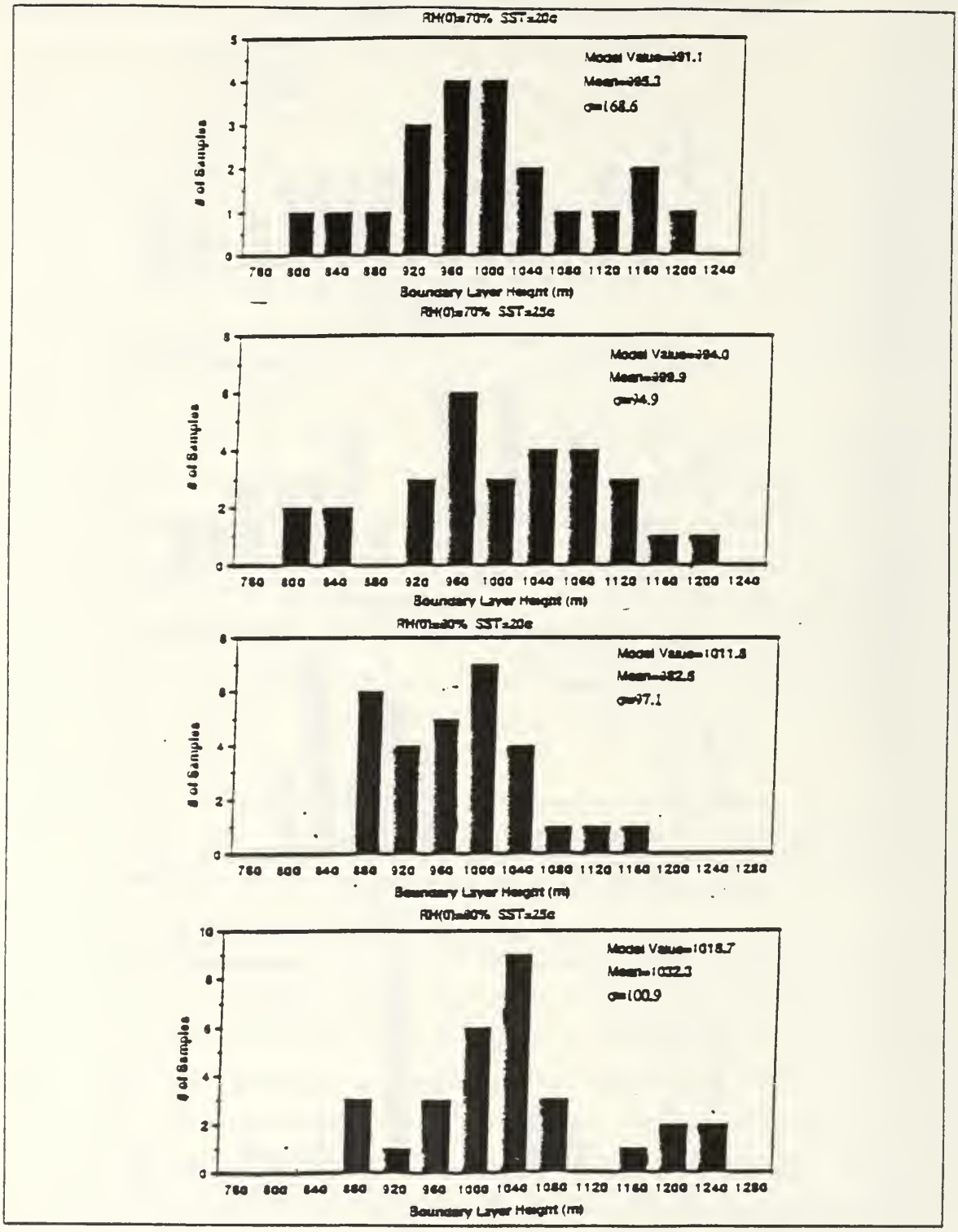

Fig. 9. Boundary layer depth histograms

TABLE 4
RH(0) AND MABL DEPTH TECHNIQUE VALUES AND t-TEST RESULTS FROM ERROR SENSITIVITY ANALYSIS

	SST (°C)	RH (%)	MIN	MEAN	MAX	MODEL VALUE
Relative Humidity (%)	20	70	65.4	68.6	71.8	69.2
	25	70	66.7	69.5	72.3	70.7
	20	80	79.0	80.2	81.4	80.3
	20	80	78.4	79.5	80.6	78.8
	25	80	77.7	78.9	80.1	78.8
Boundary Layer Height (m)	20	70	908.9	995.3	1081.7	991.0
	25	70	951.2	999.9	1048.5	994.0
	20	80	961.2	1024.0	1086.8	1014.7
	20	80	932.8	982.6	1032.3	1011.8
	25	80	980.6	1032.3	1084.0	1018.7

on extinction (optical depth) is greater, and the histogram results confirm this conclusion.

The effect of temperature on the spread of values of surface relative humidity and boundary layer depth is less evident. In both sets of histograms, the standard deviations are nearly equal when comparing the 20 and 25 °C cases. Kren (1987) points out that the technique is least sensitive to sea-surface temperature and again the histogram results support this conclusion.

The results of the t-test are presented in Table 4. The minimum and maximum values represent the range of possibilities for the mean at the 90% confidence level. The model value represents the output if a perfect measurement could be made. In all cases, the model values fell within the 90% confidence range. For example, at 25 °C and 70% surface relative humidity, the expected range of the mean of surface relative humidity for the 30 random combinations of inputs is 66.7% to 72.3%. The mean value of all 30 runs was 69.5% while more significantly the model value (70.7%), representing the "perfect" measurement, also fell within this range. For boundary layer depth at 25 °C and 70% surface relative humidity, the expected range of the mean for surface relative humidity was 951.2 m to 1048.5 m while the mean of the random combinations of inputs (999.9 m) and the model value (994.0 m) both fell within this range. For shallower boundary layer depths, the spread between the minimum and maximum values for surface relative

humidity and boundary layer depth will be lower. This is due to the previously discussed argument concerning the nonlinearity of the saturation vapor density function. From the overall results of the t-test, it can be seen that there is no significant shifting of the mean due to combined input errors.

For an atmosphere that matches the assumptions applied to the technique, estimations of surface relative humidity and boundary layer depth are within a few percent of the correct values. As the atmosphere deviates from the applied assumptions, the accuracy of the estimations will necessarily decrease. The overall results of the sensitivity study show that with the combined sensor measurement errors of the input variables of sea-surface temperature, total water vapor and optical depth, there is no significant shifting of the mean or spread in the output estimations of surface relative humidity and boundary layer depth. It must be emphasized that the study was performed under entirely simulated conditions. Technique verification and results of satellite measurements will be presented in Chapters III and IV.

III. VERIFICATION OF THE TECHNIQUE

Errors in the boundary layer depth and surface relative humidity estimates result primarily from the inaccuracies in the measurement of the input quantities of optical depth, sea-surface temperature and total water vapor (Kren 1987). Another source of error is deviation from the stated assumptions about the characteristics of the boundary layer. The verification cases presented in this chapter have ranges of total water vapor in the boundary layer from 35% to 60%. The greater the percentage of total water vapor and optical depth above the boundary layer, the greater the error in the estimates of surface relative humidity and boundary layer depth.

A. VERIFICATION METHODS

1. Satellite Data Processing

The algorithms for determination of the input variables of sea-surface temperature, optical depth and total water vapor described in Chapter II were incorporated into a program that analyzes a satellite subscene on a pixel by pixel basis. The subscenes are composed of a 512-by-512 pixel grid which corresponds to a region of approximately 600 square km and a resolution of approximately 1 km at satellite sub-point. Images of sea-surface temperature, optical depth and total water vapor were produced for each subscene and compared for consistency on a regional basis. The subscenes were also analyzed for noise in the data, usually apparent by sharp gradations between widely varying pixel counts. An area average of each input parameter was then performed on all pixels within a 0.1 degree latitude square of the desired verification point.

The verification points consisted of both research vessels and aircraft reported meteorological soundings and sea-surface temperatures. These soundings and temperatures were combined into boundary layer profiles and compared to the initial assumptions. The satellite-derived average values of sea-surface temperature, total water vapor and optical depth were then compared to the verified values. Finally, the computed estimates of boundary layer depth and surface relative humidity were compared with those generated by the ship and aircraft.

Verification of surface relative humidity values were obtained directly from the radiosonde printouts and aircraft vertical profiles. Boundary layer depth was determined by analyzing the height at which the relative humidity value decreased rapidly from a

maximum value and the atmospheric temperature began to decrease. If these occurrences were not coincident, an average height between the two was used.

2. Spatial and Temporal Differences in Technique Verification

The characteristics of the marine atmospheric boundary layer vary on the order of hours and over distances of kilometers. It is thus necessary to match as closely as possible the time of the satellite pass with the launch of the radiosondes and measurements of temperature. Dalu (1986) found that errors in water vapor retrievals increased from $\pm 0.15\ g/cm^2$ for simulated cases to $\pm 0.5\ g/cm^2$ for verification cases due to inexact spatial and temporal correlation between the ship and satellite reported locations. Spatially, the satellite-derived measurements coincided with the ship and aircraft reports in all verification cases. Temporally, every effort was made to choose cases such that the time between the two measurement techniques was less than one hour, thus minimizing a potential source of difference.

B. CASE 1; OCTOBER, 1982

The first verification test was performed on measurements taken by aircraft flights off the coast of southern California during the period 4 October through 6 October 1982. These flights were coincident with overpasses of the NOAA-7 satellite. The satellite subscene region is outlined in Fig. 10.

1. Synoptic Situation

On 5 October 1982, the southern California coastal region was dominated by a subtropical high pressure system. This resulted in a subsidence-induced inversion that capped the marine boundary layer. Fig. 11 shows the relative humidity and potential temperature profile for 33.2° N, 118.1° W at 2128 UTC on 5 October 1982. The increasing relative humidity profile and constant potential temperature from the surface to 500 m meet the assumptions for a well-mixed boundary layer. This profile corresponds to a value of approximately 60% total water vapor within the boundary layer, well below the initial assumption of all the total water vapor being confined to the boundary layer.

2. Total Water Vapor and Optical Depth Verification

Table 5 displays the results of the Case 1 verification measurements of October 1982. Only total water vapor was verified at the San Nicholas Island shore station because of the lack of sea-surface temperature data. In addition to having confirmation of total water vapor values from radiosonde reports, optical depth was compared to aircraft measurements of extinction using an Axially Scattering Spectrometer Probe (ASSP). Durkee (1984) presents a detailed description of the use of the ASSP and the

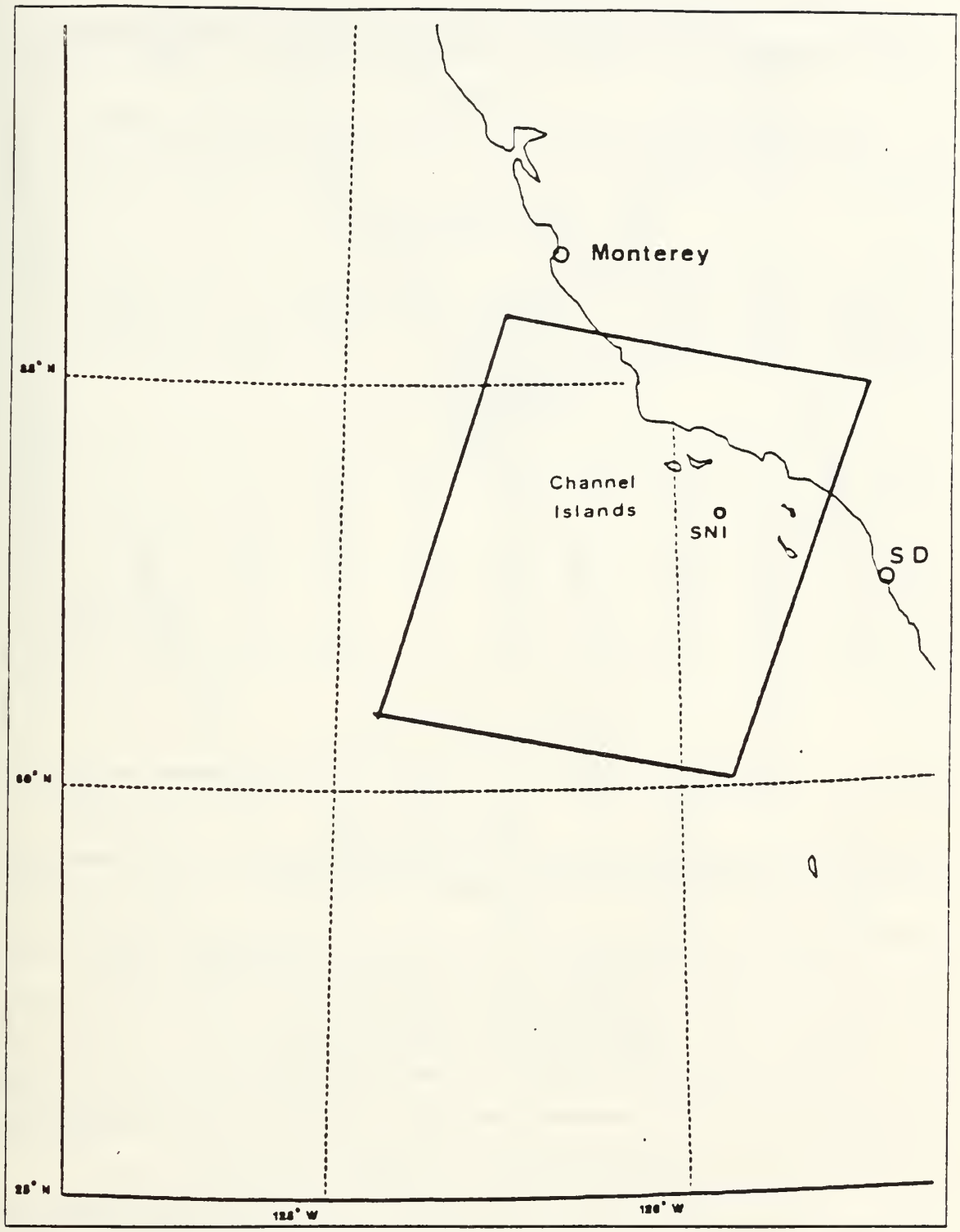

Fig. 10. Satellite subscene region for Case 1 - October, 1982

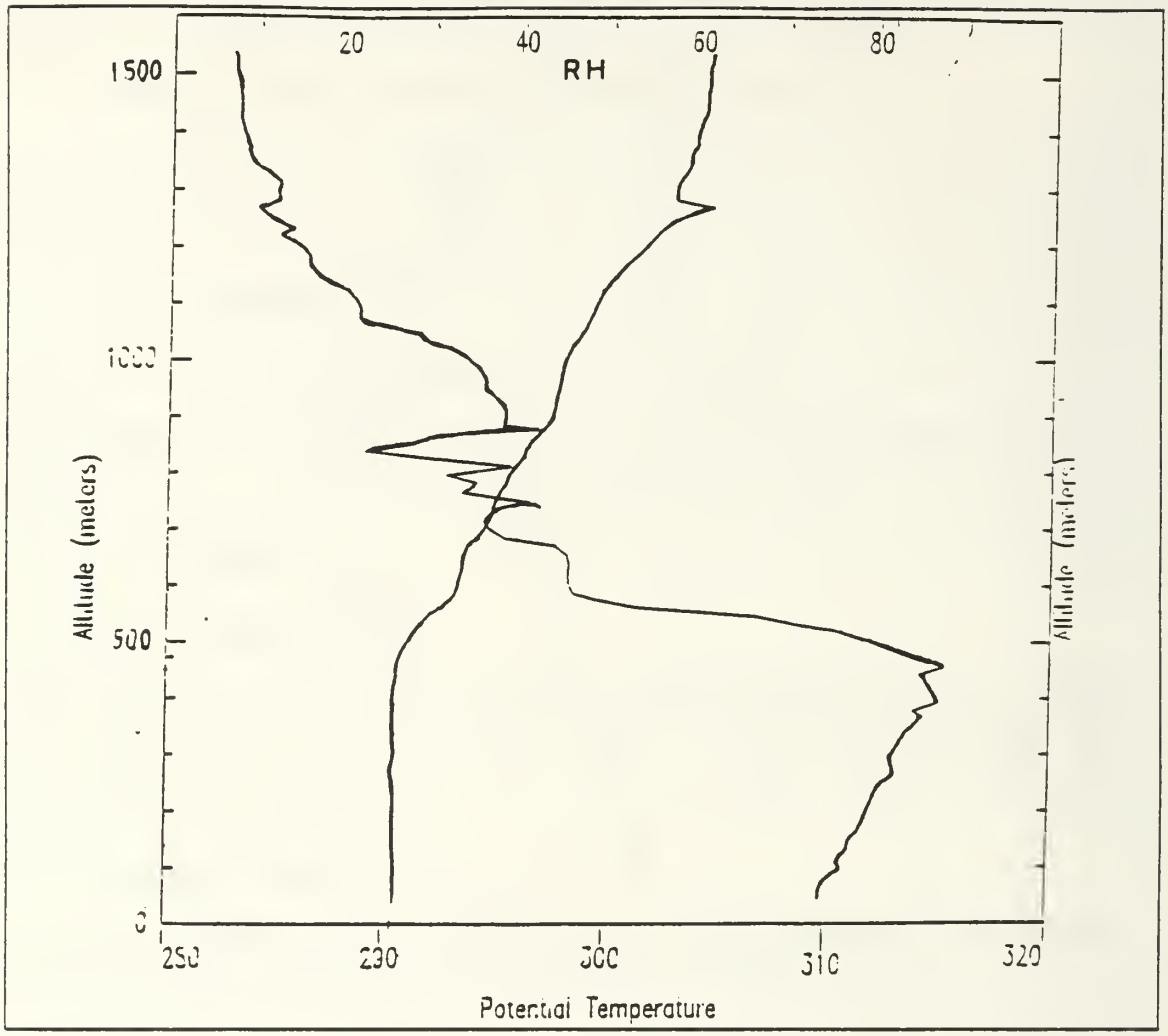

Fig. 11. **Relative humidity and θ profile: 5 October 1982**

errors inherent in determining extinction using this particular probe. While the absolute value of the extinction calculation may be accurate only to a factor of two, Jensen et al. (1980) showed that relative variations of extinction determined by the spectrometers were consistent. Since optical depth is the vertical integration of extinction, this relative comparison would also hold for optical depth. Therefore, as far as verifying optical depth, only relative comparisons between the results can be made.

October 5 and 6 were the only days in this verification study where optical depth was verified. In four of the five cases the value of optical depth was underestimated by the satellite. In the fifth case, the two values were coincident. Errors in the measurement range from .00 to .08 corresponding to an error range from zero to a factor

TABLE 5
GROUND TRUTH COMPARISON FOR CASE 1: OCTOBER, 1982

Input	Location	Ground	Sat.	Error
4 October 1982 Satellite Pass Time: 2139 UTC				
$W(g/cm^2)$	SNI	0.61	0.64	0.03
5 October 1982 Satellite Pass Time: 2128 UTC				
$W(g/cm^2)$	SNI B B1 B3	0.52 0.57 0.85 0.53	0.65 0.77 0.75 0.62	0.13 0.19 -0.10 0.09
Optical Depth	B B1 B3	0.08 0.11 0.08	0.16 0.18 0.13	0.08 0.07 0.05
6 October 1982 Satellite Pass Time: 2257 UTC				
$W(g/cm^2)$	SNI A B4	0.51 0.10 0.26	0.30 0.14 0.38	-0.21 0.04 0.12
Optical Depth	A B4	0.07 0.06	0.07 0.09	0.0 0.03
Aircraft Position at B: Lat: 33.2° N; Lon: 118.1° W B1: Lat: 33.1° N; Lon: 118.8° W B3: Lat: 33.1° N; Lon: 117.9° W B4: Lat: 33.0° N; Lon: 118.9° W SNI: San Nicholas Island Lat: 33.1° N; Lon: 119.5° W				

of two confirming the results of Jensen et al. (1980). In a relative sense, as the aircraft optical depth values increased, the satellite values of optical depth increased.

Eight cases were available to verify total water vapor, three at the San Nicholas shore station and five at the aircraft measurement points. In all cases, the error between

the satellite measured value and the radiosonde computed value was less than 0.21 g/cm^2. On the sixth of October, the satellite underestimated the value of total water vapor by 0.21 g/cm^2. As stated in the next section, every effort was made to match the satellite pass time with the radiosonde launch time. On this particular day, the satellite pass was 3 hrs and 4 min after the radiosonde launch. Dalu (1986) points out that introducing errors due to spatial and temporal measurement differences can increase the error in the retrieved value of total water vapor to $\pm 0.5\ g/cm^2$.

3. Technique Verification and Discussion

Table 6 displays the results of the verification study for the output values of surface relative humidity and boundary layer depth. Surface relative humidity verification was not available for the 4 October San Nicholas Island case because of insufficient data at the surface. In all other cases, the satellite overestimated the value of surface relative humidity by an average of 6%.

In the simulated boundary layer analysis presented in Chapter II, the standard deviation of surface relative humidity in the 80% case was 2.4%. The nearly doubled surface relative humidity error over the standard deviation value can be attributed in part to the departure from the initial assumptions. Also, the inability to accurately verify optical depth and determine the effect of continental aerosol could play a role in the results.

This is the first set of results where an apparent systematic tendency in the model is present. Kren (1987) reports that overestimates in optical depth and total water vapor taken separately produce correspondingly higher surface relative humidities.In all seven cases, either optical depth or total water vapor or both were overestimated. These overestimates are a result of the distribution of a portion of total water vapor and optical depth above the boundary layer.

The systematic tendency apparent in the surface relative humidity results was not found in the boundary layer depth results. In five of the eight cases, the satellite underestimated the value of boundary layer depth, but by relatively small amounts. The overall error in the shore station cases was 112 m and in the aircraft measured cases was 42 m. Again the difficulty in comparing shore station launches with the satellite measurements is apparent. The 42 m error in the aircraft measured cases is well within the standard deviation for boundary layer depth error from the t-test statistical analysis.

TABLE 6
TECHNIQUE COMPARISON FOR CASE 1

Location	Ground RH(0) [%]	Sat. RH(0) [%]	Error (%)	Ground Z (m)	Sat. Z (m)	Error (m)
SNI 4 Oct	-	84	-	550	521	-29
SNI 5 Oct	76	84	8	420	580	160
SNI 6 Oct	89	91	2	408	260	-48
B	75	83	8	590	574	-16
B1	77	83	6	570	593	23
B3	77	84	6	540	486	-54
A	84	95	11	130	86	-44
B4	85	87	2	220	292	72

C. CASE 2; JULY, 1987

The second verification test was performed on data taken from the First ISCCP Regional Experiment (FIRE) that was conducted off the coast of southern California from 29 June 1987 to 18 July 1987, as shown in Fig. 10. The research vessel Pt. Sur launched radiosondes and took ocean measurements concurrently with the NOAA-9 satellite passes. Also, atmospheric soundings were available from the shore stations at Vandenberg and Montgomery Field. In this particular case, total water vapor was verified at the ship and shore stations and sea-surface temperature at the ship stations. It was not possible to verify optical depth depth because of the lack of extinction measurements during the experiment.

1. Synoptic Situation

The dominant synoptic feature during the period 7-12 July for coastal southern California, shown in Fig. 12, was a surface subtropical high pressure system centered at 35.° N and 140.° W. The upper- level flow over the region was zonal throughout the period. Strong northerly winds were present along the coast producing clear conditions for approximately 100 miles seaward around the area of interest. On 9 July, the surface subtropical high intensified and moved westward, weakening the pressure gradient and the surface winds along the coast. During the period 11-12 July the high remained quasi-stationary and eventually weakened while the region directly off the coast remained clear with light winds present.

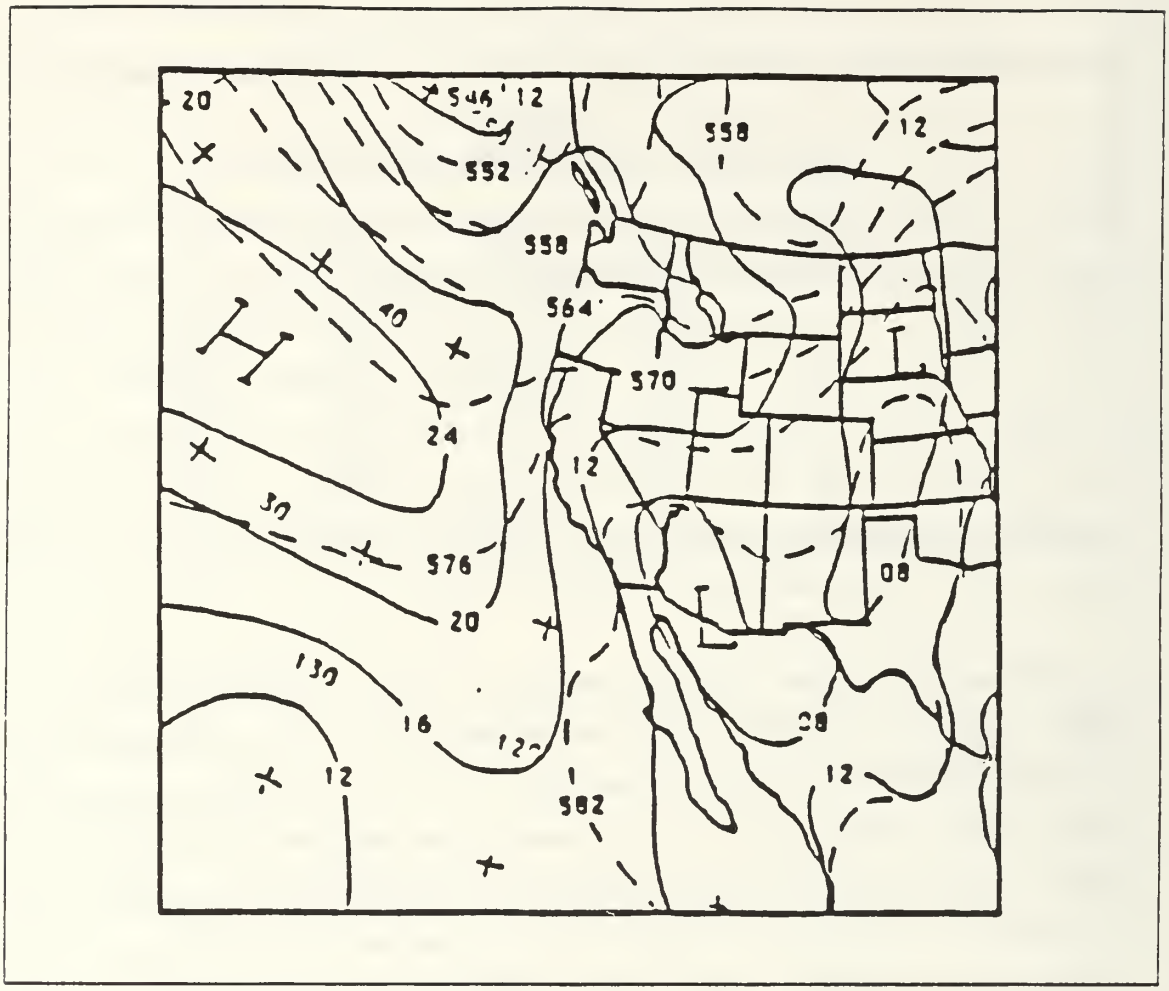

Fig. 12. Synoptic Weather Pattern for Case 2 - 7 July, 1987

As stated in the model assumptions section in Chapter II, the technique is ideally suited to open ocean regions dominated by subtropical high pressure anticyclones. Open ocean regions were not possible for these verification cases and the effect of continental aerosol on the distribution of optical depth and total water in the atmosphere remains undetermined. However, the close proximity of the subtropical high allowed for a fairly constant potential temperature profile and well-mixed boundary layer in the verification area resulting in acceptable conditions for testing the technique.

2. SST and Total Water Vapor Verification

Table 7 displays the results of the Case 2 verification measurements of July 1987. The three additional total water vapor measurements represent shore reported radiosonde launches and, as such, sea-surface temperature was not able to be verified

TABLE 7
GROUND TRUTH COMPARISON FOR CASE 2: JULY, 1987

Input	Location	Ground	Sat.	Error
7 July 1987 Satellite Pass Time: 2237 UTC				
SST(°C)	Ship	290.2	291.0	0.8
$W(g/cm^2)$	Ship	0.63	0.53	-0.10
	VBG	0.50	0.69	0.19
12 July 1987 Satellite Pass Time: 2324 UTC				
SST(°C)	Ship	288.4	288.3	-0.1
$W(g/cm^2)$	Ship	0.60	0.76	0.17
	VBG	0.47	0.35	-0.12
	MYF	0.45	0.61	0.16

7 July 1987: Ship Lat: 33.6° N; Lon: 120.2° W
12 July 1987: Ship Lat: 33.3° N; Lon: 120.0° W
MYF: Montgomery Field Shore Station Lat: 32.8° N; Lon:117.1° W
VBG: Vandenberg Shore Station Lat: 34.7° N; Lon:120.6° W

at these locations. Looking first at sea-surface temperature, the errors are well within the 1.1 °C error reported by McClain (1985). Taken alone, these errors would correspond to errors in the surface relative humidity and boundary layer depth of less than 3% and 40 m respectively, based on the sensitivity study conducted by Kren (1987).

For total water vapor, the ship reported W represents the amount of total water in the boundary layer only. The amount of total water vapor in the boundary layer was determined by vertically summing the value of vapor density over the entire atmospheric column. By analyzing the radiosonde report, a determination of the height of the boundary layer can be made and then used to identify the amount of total water within it. In all cases, the total water for the entire atmospheric column was above 2.0 g/cm^2 but the comparison in Table 5 is made between the satellite reported total water vapor

and that amount of W within the boundary layer, consistent with the initial assumptions. The average amount of total water vapor within the boundary layer for these cases is approximately 35%. Even with this apparent gross deviation from the assumption about the distribution of total water in the boundary layer, errors in the measured amount ranged from 0.10 to 0.19 g/cm^2 , on the order of those reported by Dalu (1986). Taken alone, these errors would correspond to errors in surface relative humidity and boundary layer depth of approximately 5% and 100 m respectively based on the sensitivity study conducted by Kren (1987). There appears to be no systematic tendencies in the errors of both SST and total water vapor, as there are underestimates and overestimates made by the technique in both parameters.

3. Technique Verification and Discussion

The input measurements listed in Table 7 along with the satellite derived values of optical depth were used in the model to produce estimates of boundary layer depth and surface relative humidity. The results are presented in Table 8. Errors in surface relative humidity average 9% and in boundary layer depth average 187 m. It is necessary to separate the ship results from the shore station results. Points directly offshore from the Vandenberg (VBG) and Montgomery Field (MYF) stations were used in order to get valid sea-surface temperature and total water vapor measurements. This induces a spatial error that certainly affects the results. The average surface relative humidity error (9%) was equal to the ship case errors but the boundary layer depth was significantly greater (245 m vs. 98 m). The spatial disparity induces errors in all three satellite measured variables of sea-surface temperature, total water vapor and optical depth with the most significant being optical depth. As stated in Chapter II, the effect of continental aerosol on the total amount of Mie scattering and thus optical depth remains undetermined at this point.

For the 7 July ship case, the 9% underestimate in surface relative humidity is well above the average standard deviation of 3.5% from the histogram results presented in Chapter II. The satellite estimated value of total water vapor was 0.10 g/cm^2 less than the actual value, which by itself would tend to greatly underestimate the surface relative humidity. The boundary layer depth error of 73 m is well within the average standard deviation of 115 m from the histogram results and represents a 10% error in the estimate of the MABL depth in this case.

For the 12 July ship case, the technique underestimated the boundary layer depth by 123 m. This case contained the greatest error in total water vapor estimation

TABLE 8
TECHNIQUE COMPARISON FOR CASE 2

Date Place	Ground RH(0) [%]	Sat. RH(0) [%]	Error (%)	Ground Z (m)	Sat. Z (m)	Error (m)
7 July Ship	96	87	-8.7	780	707	-73
7 July VBG	72	85	13	510	680	170
12 July/VBG	85	90	5	450	130	-320
12 July/ Ship	76	84	8	570	447	-123

(0.17 gm/cm^2) which was apparently manifested in the large error in boundary layer depth.

These results must be looked at in relation to the initial assumptions. In both cases, the majority of the total water vapor was above the boundary layer, violating a major assumption. The technique still produced reasonable results for both surface relative humidity and boundary layer depth. The relatively large errors in surface relative humidity and boundary layer depth for the shore cases could be the result of several factors. Certainly the violation of the assumption of total water vapor in the boundary layer is significant. Equally important could be the previously mentioned errors in spatial measurements in the shore station cases. Finally, the inability to verify optical depth for these cases and determine the amount of continental aerosol above the boundary layer makes it impossible to assess the effect of measurement errors in this parameter.

D. COMPOSITE VERIFICATION RESULTS

1. Total Water Vapor Comparison

The first three sections of this chapter delineated verification results for separate synoptic situations. This was done in order to assess the effect of differing atmospheric conditions on the magnitude of the error of the input parameters. The lack of enough sea surface temperature comparisons and the inability to accurately account for the absolute magnitude of optical depth leaves total water vapor as the one input parameter on which a correlation can be made with the outputs of surface relative humidity and boundary layer depth. Since total water vapor is the most sensitive of the three inputs on estimates of surface relative humidity and boundary layer depth (Kren, 1987), the corresponding cause and effect relationship presented here is the most significant.

Table 9 shows the errors in total water vapor in the two synoptic cases and the effect on output values. one of the three errors that must be taken together, the high sensitivity of the model to errors in W make the comparison reasonable. The increase in the percentage of total water vapor (and most likely optical depth) in the boundary layer from Case 1 to Case 2 is manifested in the reduced errors in both the total water vapor estimations and the output estimations of surface relative humidity and boundary layer depth. A modest 25% increase in the amount of total water vapor in the boundary layer correlates with reductions in the surface relative humidity error by a factor of 1/3 and the boundary layer height error by a factor of 2/3.

2. Composite Scattergrams

One method of evaluation of composite data results is the use of scattergrams that display verification/satellite measurement points from all cases. Fig. 13 on page 40 shows scattergrams for surface relative humidity and boundary layer depth. In the surface relative humidity scattergram, there is a strong bias toward the satellite overestimating the correct verification value. As stated in Chapter II, overestimates of total water vapor and optical depth produce a compensating effect, optical depth increasing the surface relative humidity and total water vapor decreasing the surface relative humidity. However, the overestimate of optical depth in these cases appears to have dominated, producing overestimates of surface relative humidity.

The estimates of boundary layer depth do not show the same bias. The standard deviation of 55 m compares favorably with the average standard deviation of 115 m from the histogram results from Chapter II.

TABLE 9
EFFECT OF ERRORS IN TOTAL WATER VAPOR CONTENT CONTENT ON OUTPUT VALUES

Case	% W in Layer	$\overline{W}_{error}$	$\overline{RH}_{error}$	$\overline{Z}_{error}$
July 1987	35%	.15	9%	188m
October 1982	60%	.11	6%	56m

The necessity to verify satellite estimations of sea surface temperature, total water vapor and optical depth and ultimately surface relative humidity and boundary layer depth cannot be overemphasized. Simulated results certainly serve a purpose but the technique advanced in this thesis relies on actual satellite measurements as a final test of validity. The results presented here verify the applicability of the technique under actual conditions within a reasonable range of error. Chapter IV will highlight the final product of the technique, synoptic scale images of surface relative humidity and boundary layer depth.

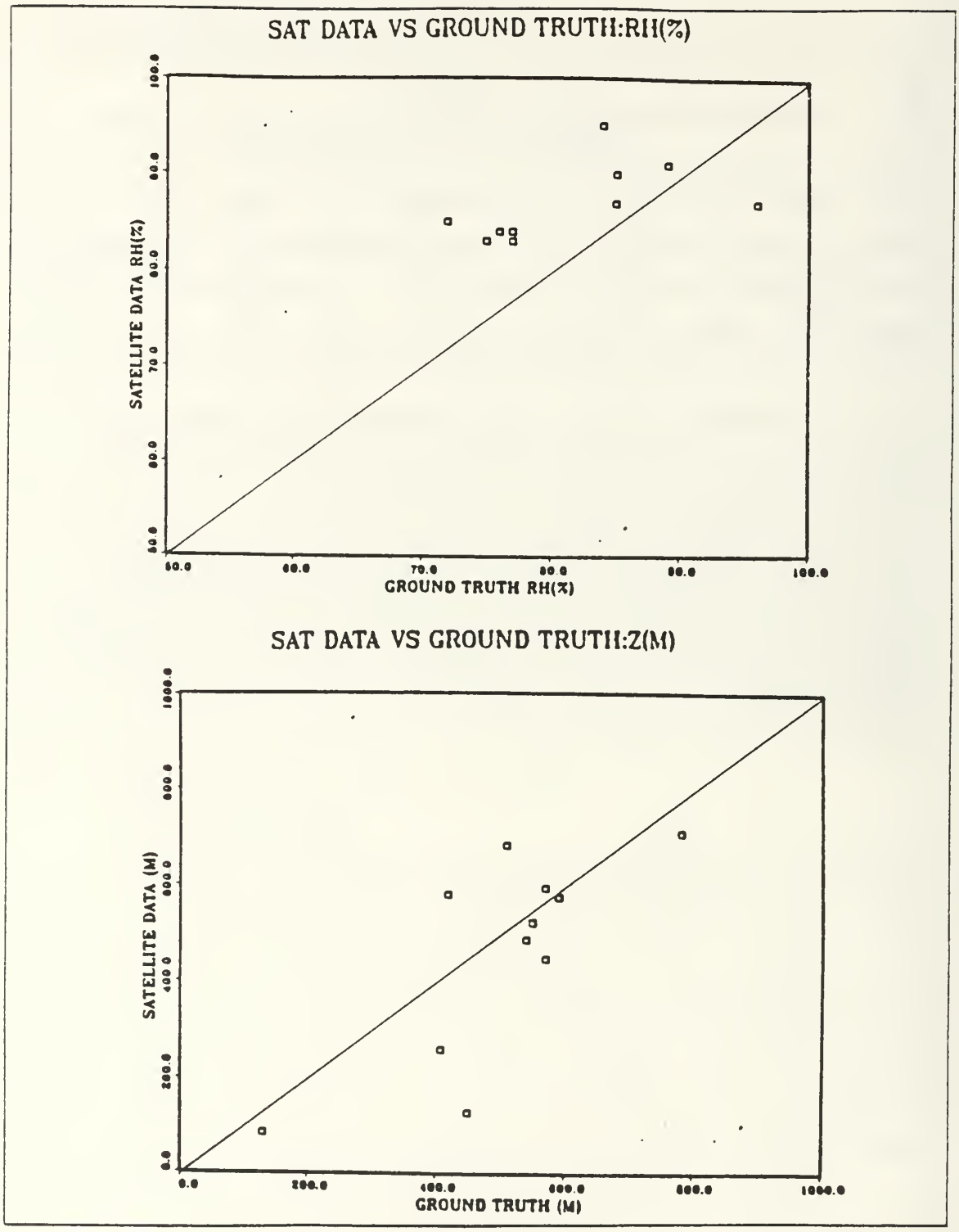

Fig. 13. Scattergrams For RH(0) and Z

IV. SURFACE RELATIVE HUMIDITY AND BOUNDARY LAYER HEIGHT IMAGES

The results presented here represent a first attempt at estimating surface relative humidity and boundary layer depth of the MABL on a large-scale basis. As pointed out in previous chapters, the technique is limited in scope to cloud free conditions and regions where the measurements of sea-surface temperature, optical depth and total water vapor are meteorologically consistent. The purpose of producing surface relative humidity and boundary layer depth images is to graphically illustrate the horizontal variability of the boundary layer on a synoptic scale. These images then can be related to the air-sea dynamics that produce the variability, and a greater understanding of the physics occurring in the boundary layer can be achieved.

A. SEQUENCE OF EVENTS TO PRODUCE AN IMAGE

Fig. 14 outlines the steps involved in the technique developed in this thesis from initial input measurements of sea-surface temperature, total water vapor and optical depth to final color enhanced images of surface relative humidity and boundary layer depth.

The first step is to check for cloud contamination using the channel 1 (0.63 μm) reflectance value. The reflectance of the cloud free ocean as measured at a satellite is generally less than 10% (McClain, 1985). Comparison of shipboard measurements of sea-surface temperature and total water vapor with satellite derived measurements has shown that 15% is a reasonable cutoff for cloud contamination. Errors in cases where the reflectance approached 15% were less than 1.0 °C in sea-surface temperature and 0.10 gm/cm^2, within the measurement errors reported by McClain (1985) and Dalu (1986) respectively. Those pixels that have reflectances greater than 15% are automatically removed from the sequence and imaged as black. The effect of high reflectance values on measurements of all the input parameters is to overestimate them such that the errors exceed an acceptable amount for use in the technique.

If the reflectance is less than 15%, the algorithms for measuring the variables of sea-surface temperature, total water vapor and optical depth are invoked. These inputs plus an initial value of the relative humidity lapse rate, C = to 14.07 %/km are then used

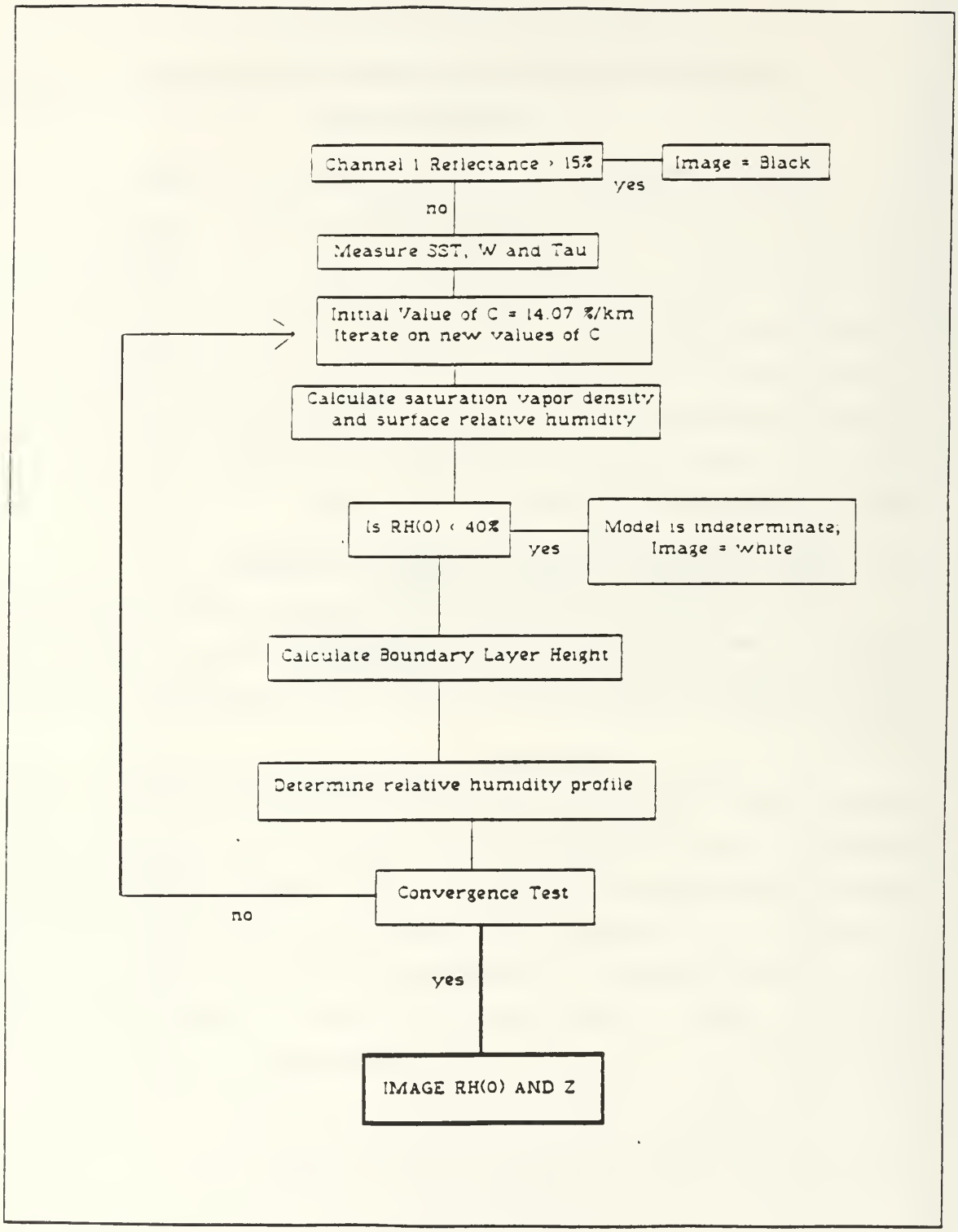

Fig. 14. Sequence of Events to Produce an Image

to calculate an initial saturation vapor density, surface relative humidity and boundary layer depth using Eqs. 12 and 14.

The iteration process is a three-step sequence that culminates in a revised value of the relative humidity lapse rate based on an improved estimate of boundary layer height First, the technique determines if the relative humidity will reach the maximum value of 97% anywhere within the layer. If this occurs, a 97% relative humidity is assumed from that point to the top of the layer as shown in Fig. 6. The technique then computes a surface relative humidity and boundary layer depth based on Eqs. 16 and 17 which balance the input variables in a manner consistent with the assumed 97% relative humidity profile case. The technique checks to see if saturation is again reached within the layer once the new estimations of surface relative humidity and boundary layer depth have been computed by utilizing Eq. 9 and substituting 97% for RH(z) and solving for Δz:

$$\Delta z = \frac{97 - RH(0)}{C}. \tag{21}$$

If the value of Δz from Eq. 21 is less than the previously computed value of boundary layer depth, the technique again assumes a saturated layer and iterates on Eqs. 16 and 17. Each time a surface relative humidity and boundary layer estimation is computed, Eq. 21 is invoked to test for saturation within the layer. Iteration and convergence occurs when the difference between two successive values of boundary layer depth is less than one meter.

If the surface relative humidity drops below 40% during any step in the iteration process, the coefficients for the imaginary portion of the quadratic equation to solve for RH(0), (Eq. 17), are non-zero and the technique is inconclusive for that pixel. If this occurs, there is no further processing and the pixel is assigned a value corresponding to white on the monochrome image. The image for surface relative humidity is scaled for a grey shade range of 0 to 255 corresponding to a humidity range of 40% to 97%. The image for boundary layer depth is also scaled scaled from 0 to 255 corresponding to a range of 0 to 2000 m.

B. OCTOBER 1982 IMAGES

The 6 October 1982 case was chosen to detail the imaging sequence from raw reflectance values to final surface relative humidity and boundary layer depth values. Fig. 15 shows the monochrome image of channel 1 (0.63 μm). Low cumulus clouds are

Fig. 15. Visible image for 6 October 1982

evident in the bottom of the image south of the channel islands off the coast of southern California. High cirrus clouds are also present in the upper left corner of the image. The regions of cumulus clouds will be masked by selective filtering in the optical depth, surface relative humidity and boundary layer depth images. In the previous section, the method for cloud filtering was described where pixels with channel 1 reflectances greater than 15% are removed from the sequence. This works well with cumulus clouds with high moisture content, but it is possible for some cirrus-contaminated pixels to pass the 15% reflectance test. In these instances it has been found that the technique is not able to converge on a solution for surface relative humidity using Eqs. 19 and 20 in the saturated layer case and these pixels are imaged as white.

Fig. 16 shows the sea-surface temperature field derived from channels 4 (10 μm) and 5 (13.0 μm), discussed in Chapter II. The range of temperatures is relatively small, 12 °C, corresponding to yellow on the image and 21 °C corresponding to the dark red. The coldest temperatures are found in the northern coastal waters, probably due to upwelling of colder, deeper water while the warmest temperatures are found in the southern California region.

Fig. 17 shows the image of total water vapor produced using the methods described in Chapter II. The red corresponds to low total water vapor values and the blue to high total water vapor values. The lowest total water vapor values are found in the same north-south band described above around the channel islands. Generally, total water vapor increases moving from the coast to the open ocean. The cirrus clouds in the upper left corner are characterized by high total water vapor content indicating a portion of the total water vapor is found above the boundary layer.

Fig. 18, the image for optical depth, was created using reflectance values from channel 1 in the visible spectrum. Completely black regions again are where the channel 1 reflectance is greater than 15%. The values for optical depth range from 0.1 to 0.75 with the lower optical depths present along the coast and higher optical depths over the open ocean. The highest optical depth values, imaged as white, are coincident with the edges of both the cirrus and cumulus clouds.

Fig. 19 is the 6 October 1982 color enhanced image of surface relative humidity. As described in the previous section, the region of high cirrus passed the channel 1 reflectance test but was imaged as white because of the inability to converge to a solution of surface relative humidity using Eq. 17.

Fig. 16. Sea surface temperature image for 6 October 1982

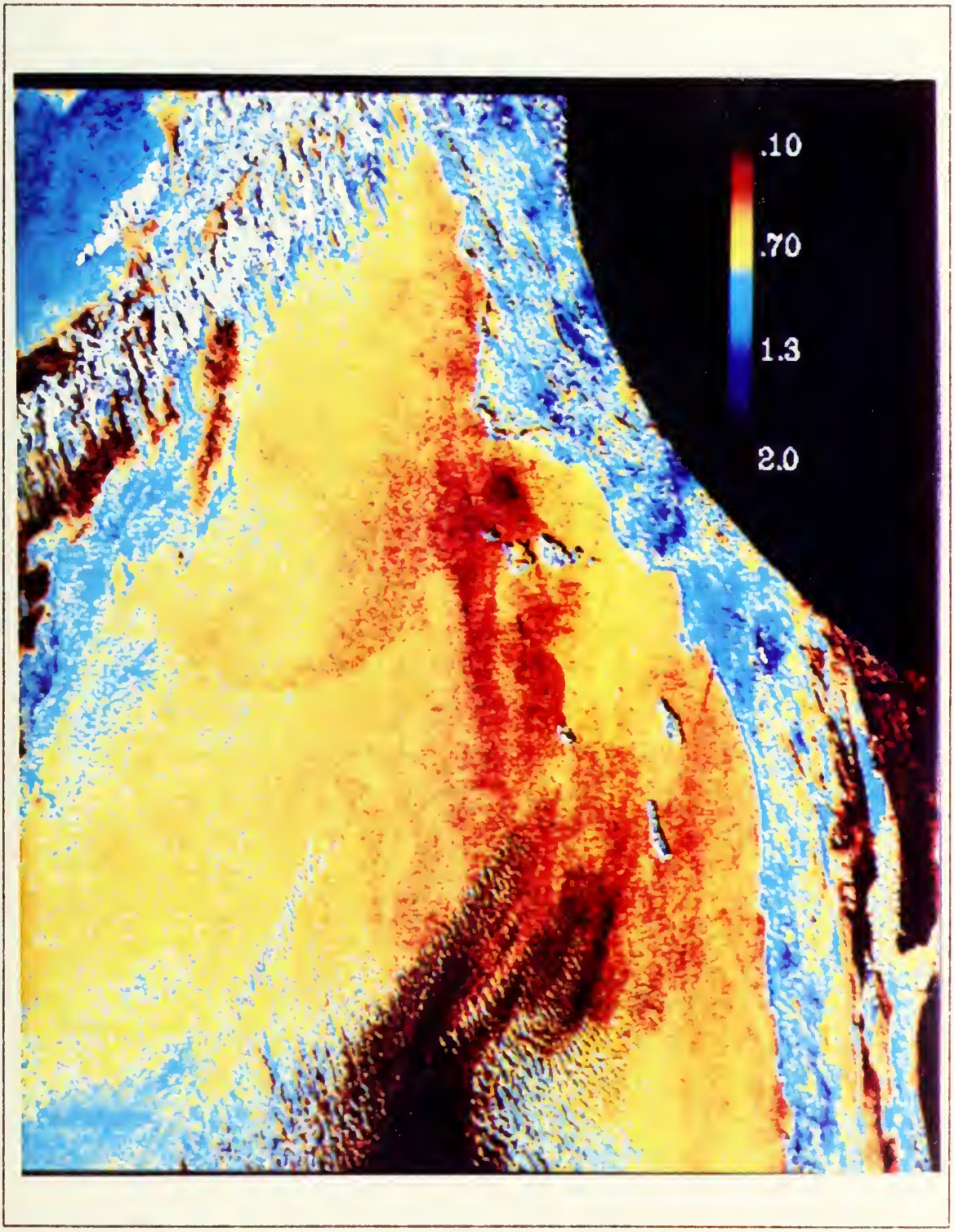

Fig. 17. Total water vapor image for 6 October 1982

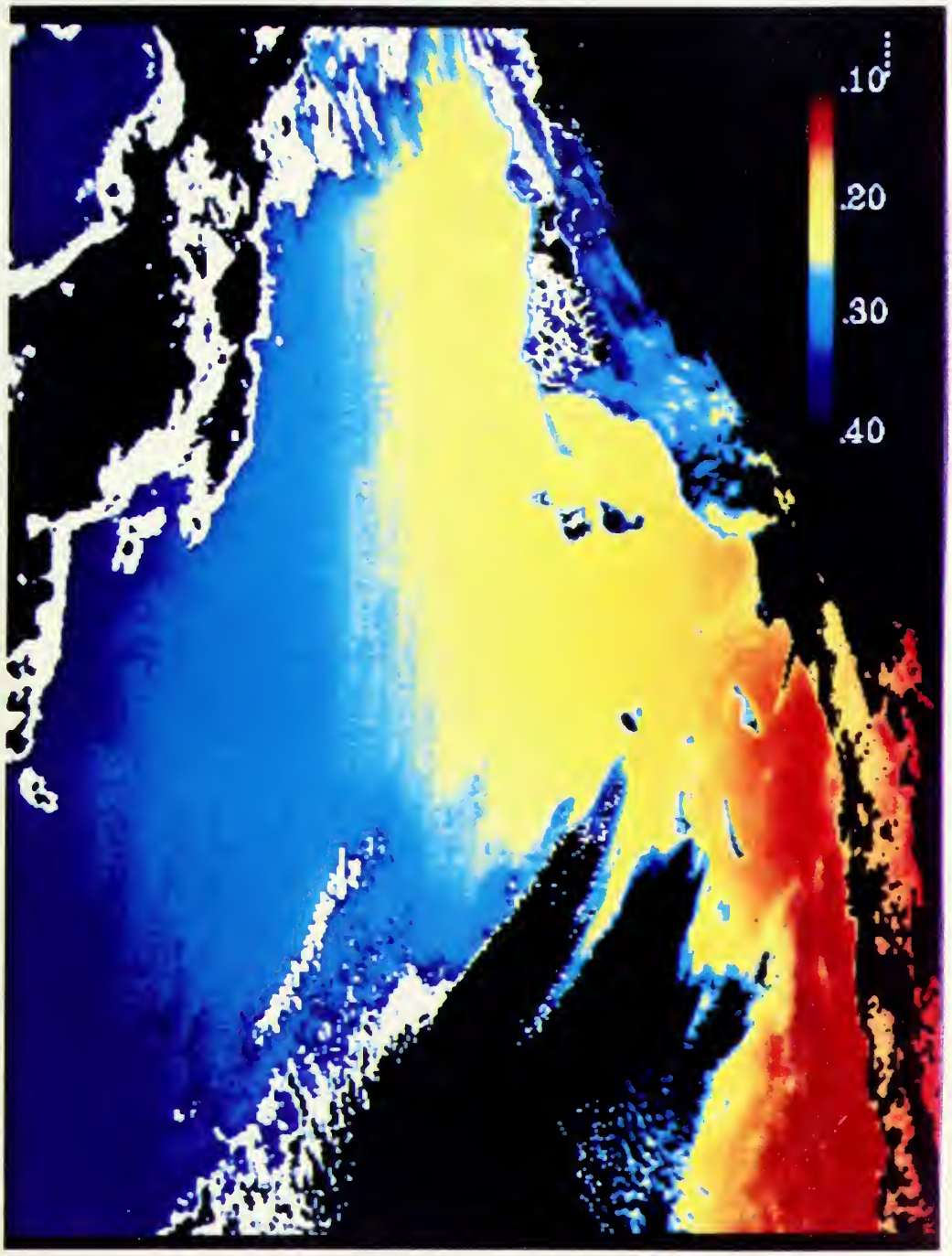

Fig. 18. Optical depth image for 6 October 1982

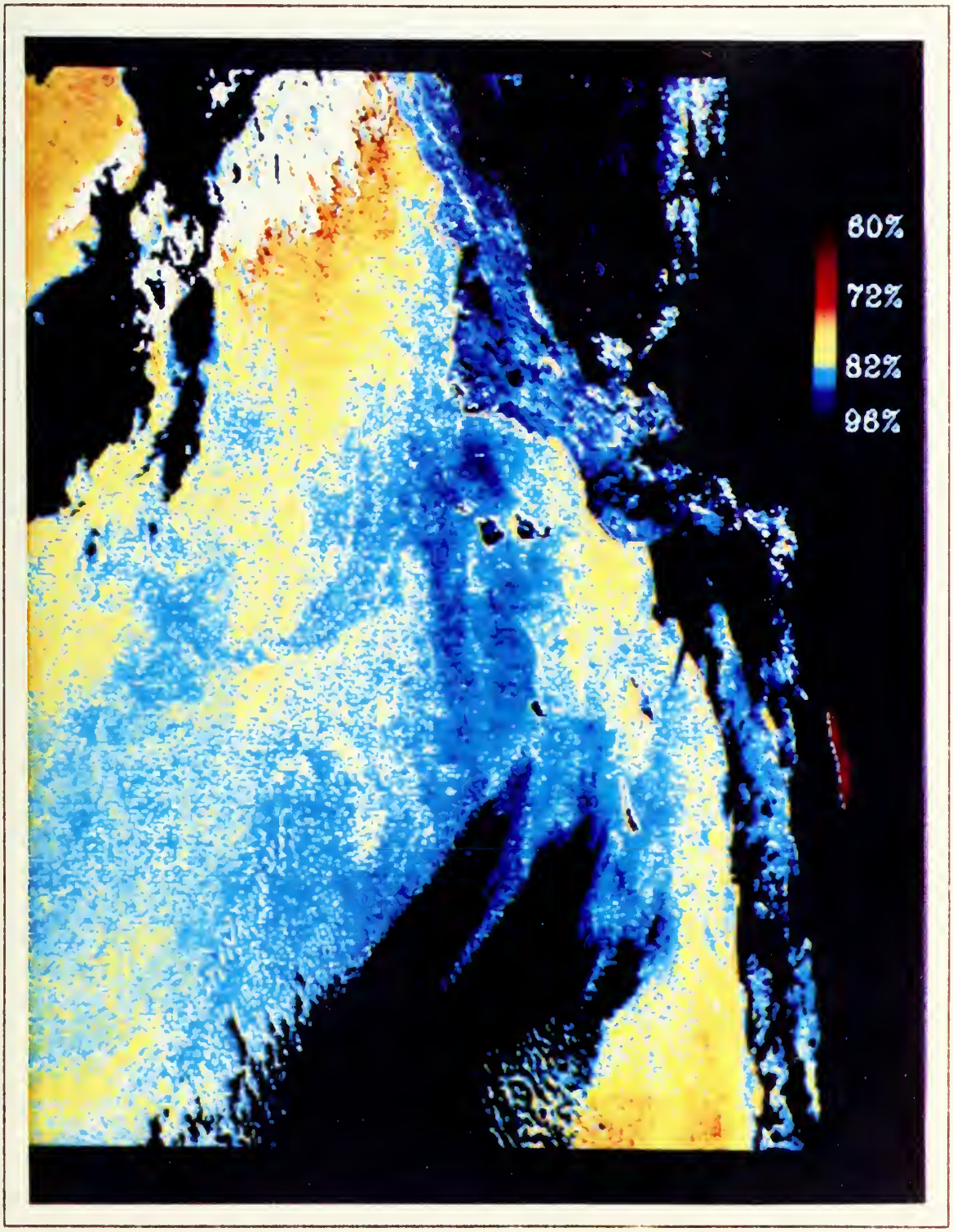

Fig. 19. Surface relative humidity image for 6 October 1982

The range of values for surface relative humidity in this case is from 75% (red) to 94% (blue). Several interesting features are present. First and most important is the regional variability in surface relative humidity down to a resolution of several kilometers. As stated earlier, the resolution of the AVHRR sensor at satellite sub point is approximately 1 km which corresponds to 1 pixel. Variations in surface relative humidity values over the span of a few pixels are easily detectable, indicating the surface relative humidity changes significantly over the range of a few kilometers. This process represents the first attempt to map the surface relative humidity field on a synoptic scale from satellite measurements.

The relatively low surface relative humidity values in the bottom of the image in Baja California and the Salton Sea are a result of the warmer surface temperatures and correspondingly higher saturation vapor densities in the surface layer. The highest surface relative humidities are found at the edges of the cumulus clouds and also just offshore around the channel islands.

Fig. 20, the boundary layer depth image, shows the lower boundary layer depths as red (300 m) and the higher boundary layer depths as blue (1600 m). As in the surface relative humidity image, variations in boundary layer depth values occur over the range of a few kilometers. The correlations between the input variables of sea-surface temperature, total water vapor and optical depth with surface relative humidity also hold for boundary layer depth.

Because of the complexities in the interrelationship between surface relative humidity, boundary layer depth, sea-surface temperature, optical depth and total water vapor, there is no strong correlation between surface relative humidity and boundary layer depth. However, in general, lower surface relative humidity is found in regions of deeper boundary layer depths. This is because of the relationship between relative humidity and extinction, discussed in Chapter II. A decrease in surface relative humidity leads to a decrease in the humidity for the boundary layer. This decrease in the humidity corresponds to a decrease in extinction. Since optical depth is a fixed quantity, the decrease in extinction through lower boundary layer humidities leads to an increased estimate of boundary layer depth (Kren, 1987). Since the assumed relative humidity profile increases with height, lower surface relative humidities allow for deeper boundary layer depths prior to saturation. Again, this is a generalization, as there are some areas of high surface relative humidity corresponding to deep boundary layer depths and vice versa.

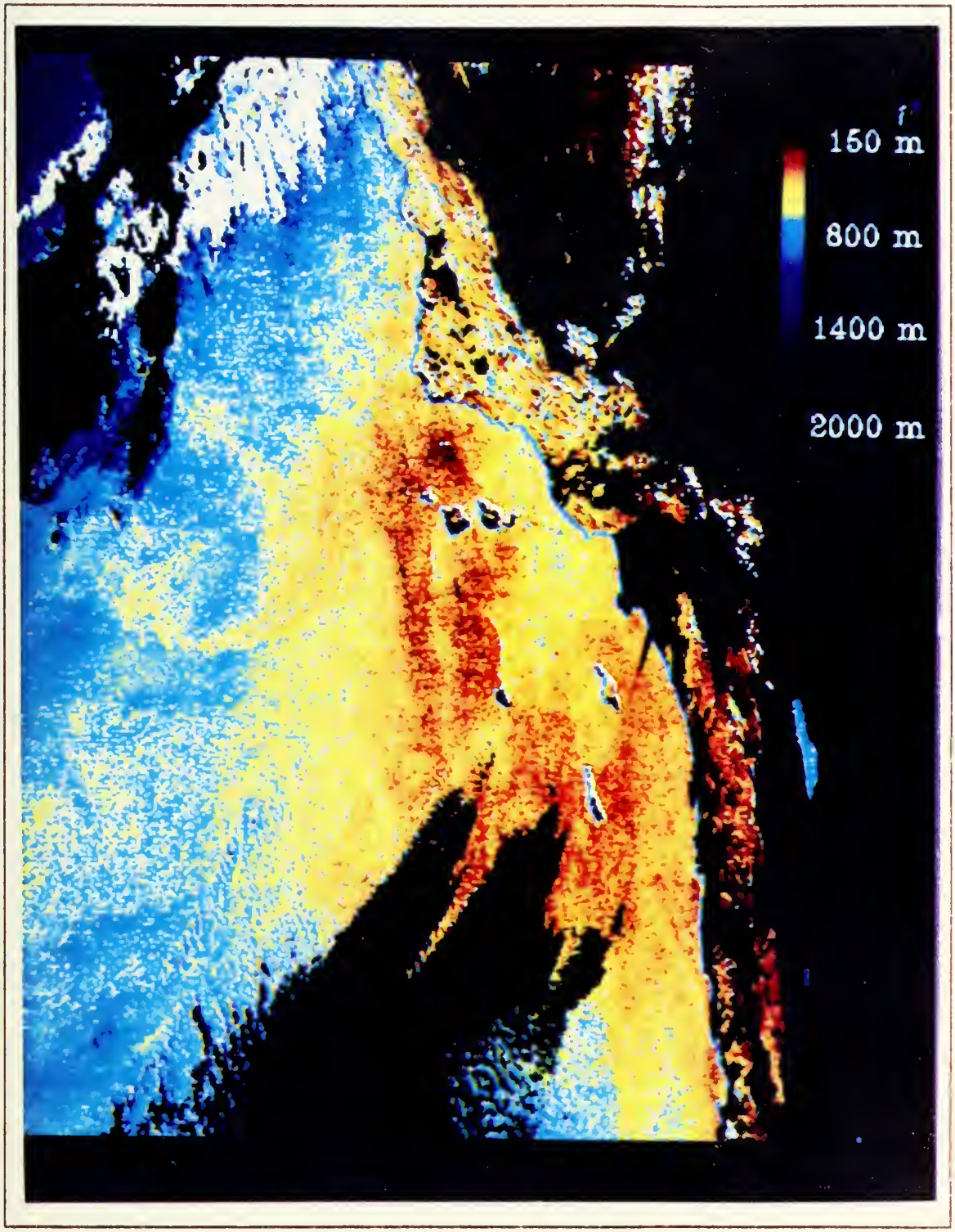

Fig. 20. Boundary layer depth image for 6 October 1982

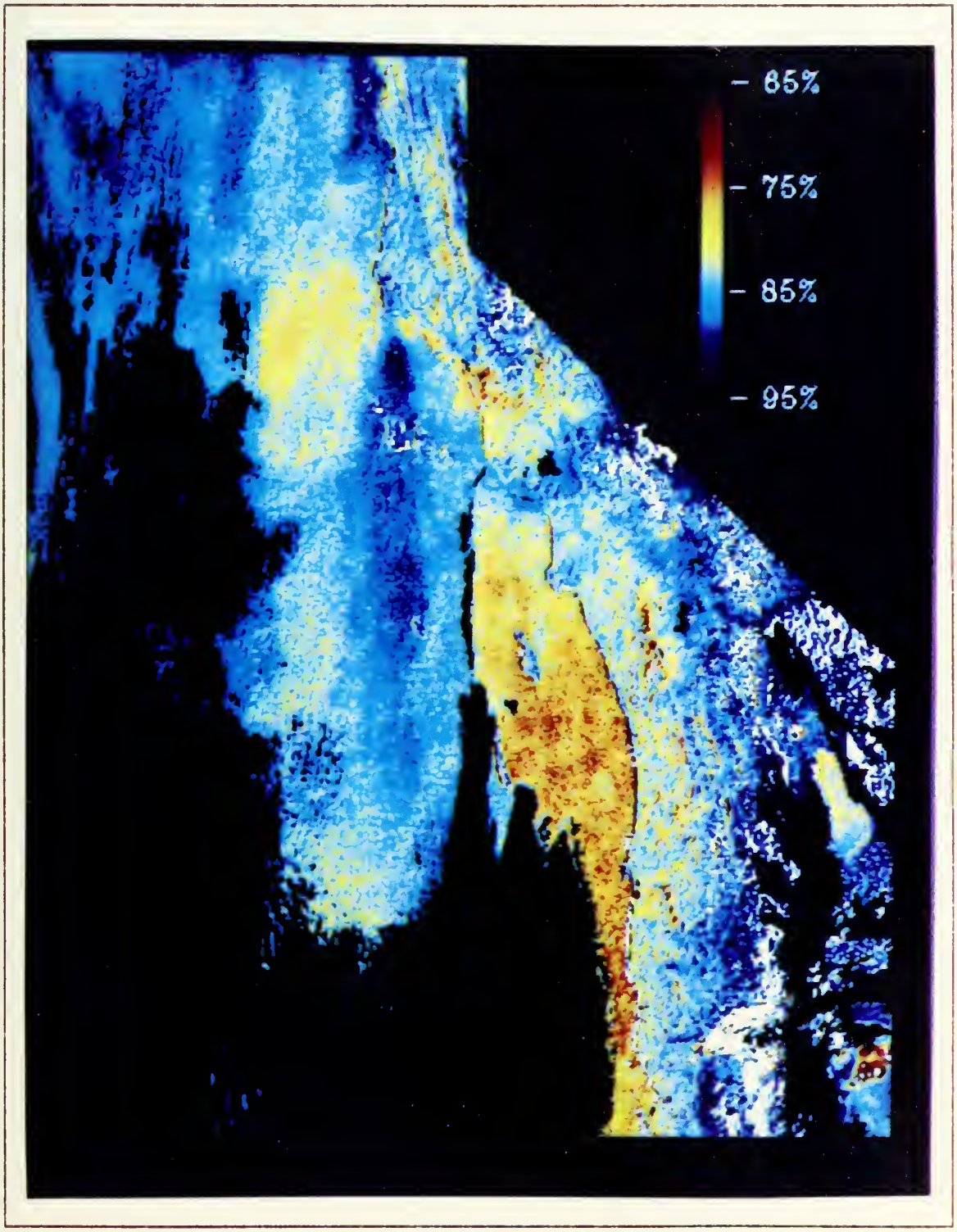

Fig. 21. Surface relative humidity image from 4 October 1982

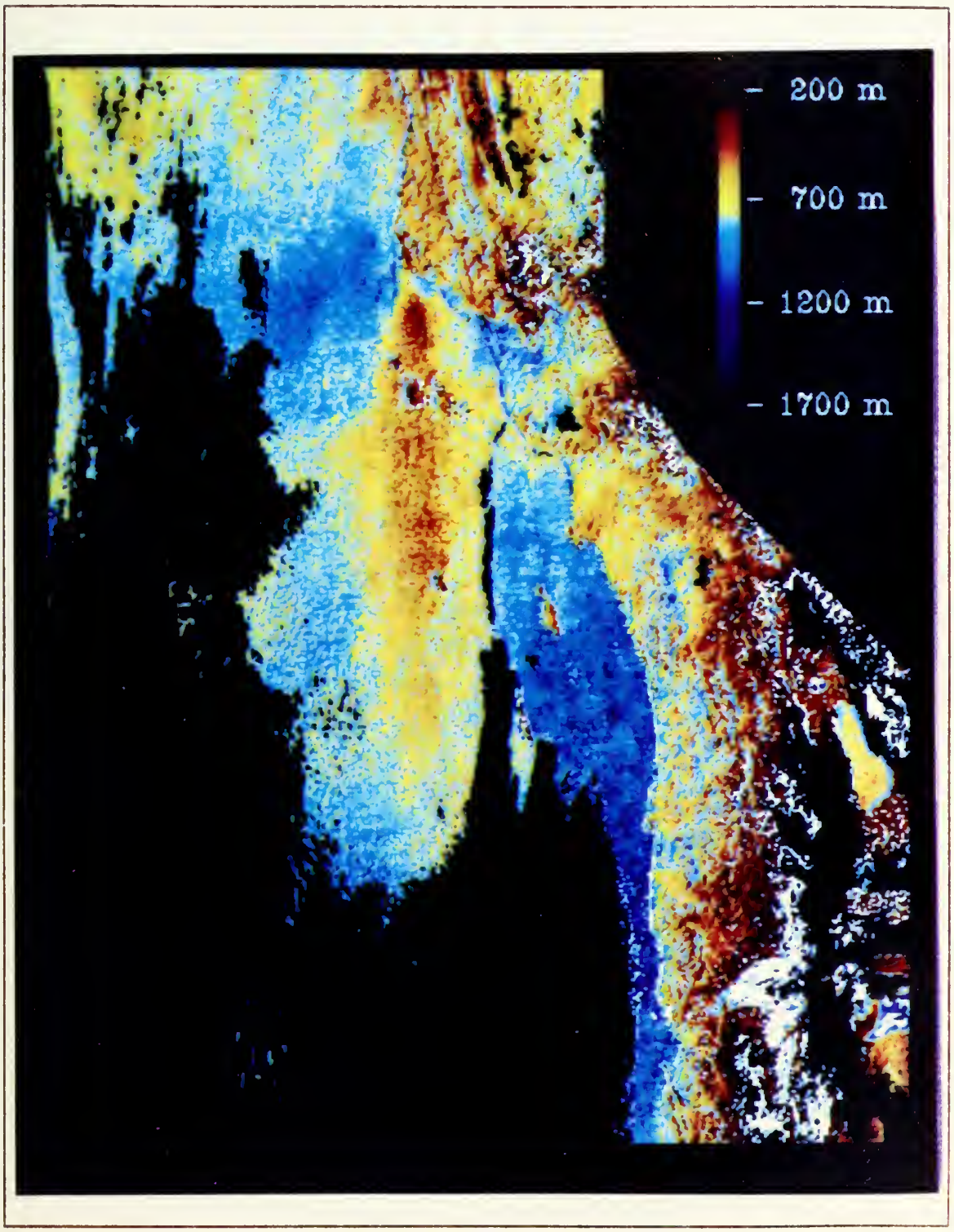

Fig. 22. Boundary layer depth image from 4 October 1982

The satellite pass for 4 October 1982 placed the coast of California on the far western portion of the image. This forced the area of usable data to be relatively small and confined to the coast from Point Conception south to Baja, California, as shown in Fig. 21. The coastline can be identified as a red and white line separating the lower near-shore surface relative humidities in red and orange from the California coast, mostly in blue. There is a distinct gradient between surface relative humidities of 85% to 95% offshore and humidities of 70% to 80% in the near shore region around the channel islands. The Salton Sea, in the lower right corner, also shows relatively low surface relative humidities, in the 75% range, similar to the 6 October 1982 case.

The strong gradient between surface relative humidities is also present in the boundary layer depth image for 4 October 1982, shown in Fig. 22. The near-shore region has boundary layer depths from 800 m to 1200 m while the region around the channel islands has depths of 400 m to 700 m. It is interesting to note the thin cloud line that separates the two regions of differing values in both the surface relative humidity and boundary layer depth images.

The 5 October 1982 surface relative humidity image is shown in Fig. 23. This satellite pass also covered only the near-shore southern California region. Again a very noticeable gradient between surface relative humidities of 70% to 80% near the shore and humidities of 90% westward of the channel islands is present. Strong offshore winds were present during this time period and warm thermal advection could cause the near-shore surface relative humidities to decrease.

In Fig. 24, very low boundary layer depths, on the order of 300 m correspond to the high surface relative humidities west of the channel islands. Cirrus clouds are present along the southern California coast and west of the Salton Sea. The horizontal black line in the lower portion of the image indicates a single line of unusable satellite data.

C. IMAGES FROM JULY 1987 CASES

The cases from the FIRE data of 7-12 July 1987 had significant cumulus and stratus cloud formations throughout the period. This necessarily limited the applicability of the technique to a relatively small region surrounding the channel islands. Nevertheless, there is a noticeable variation in the surface relative humidity image, Fig. 25. The California coastline is evident in the upper portion of the image as a distinct boundary between blue pixels and yellow pixels. In the southern part of the image surrounding Santa Catalina Island, surface relative humidities ranged from 78% to 88%. Strong northerly winds were present throughout the time period and warm thermal advection

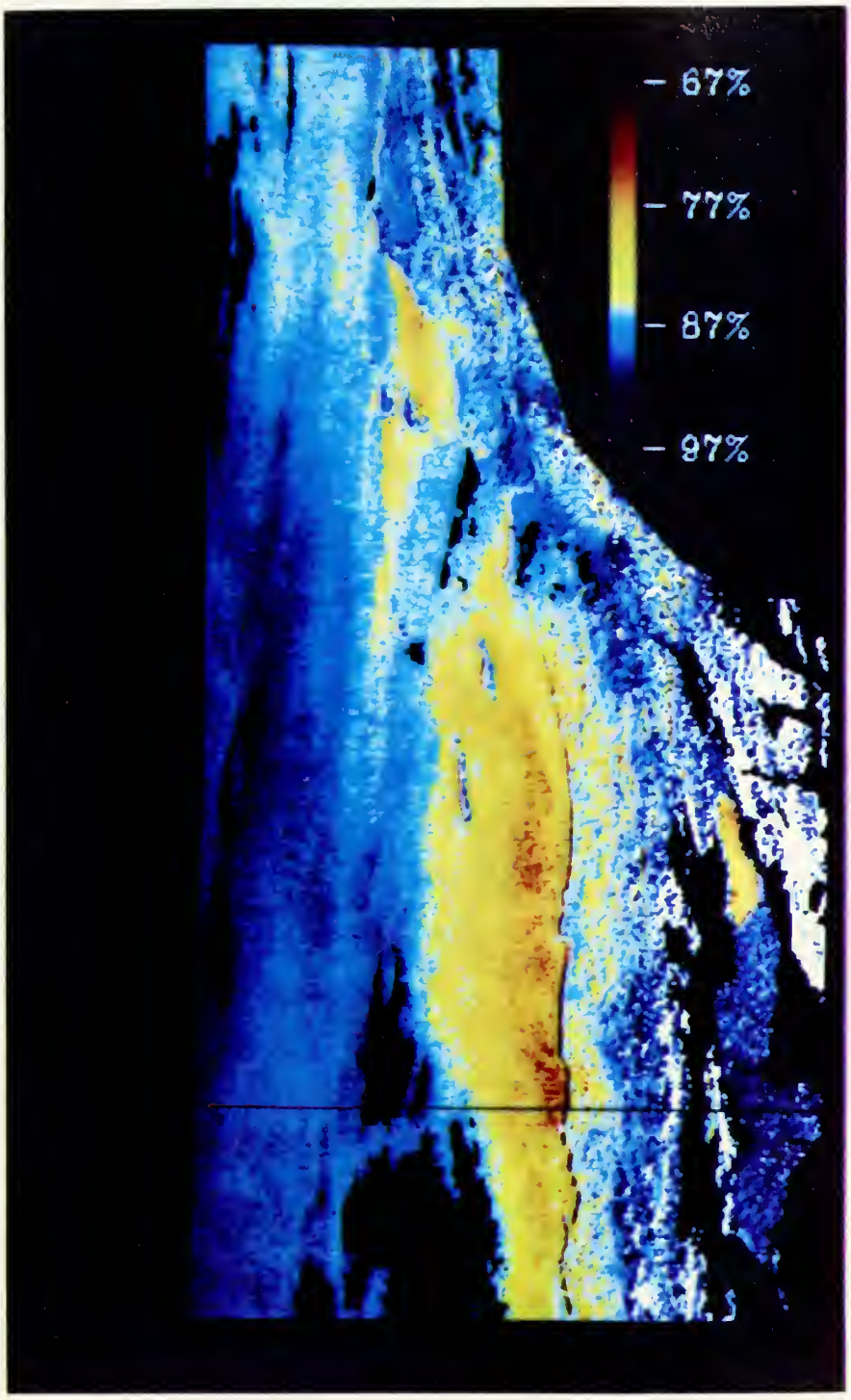

Fig. 23. Surface relative humidity image from 5 October 1982

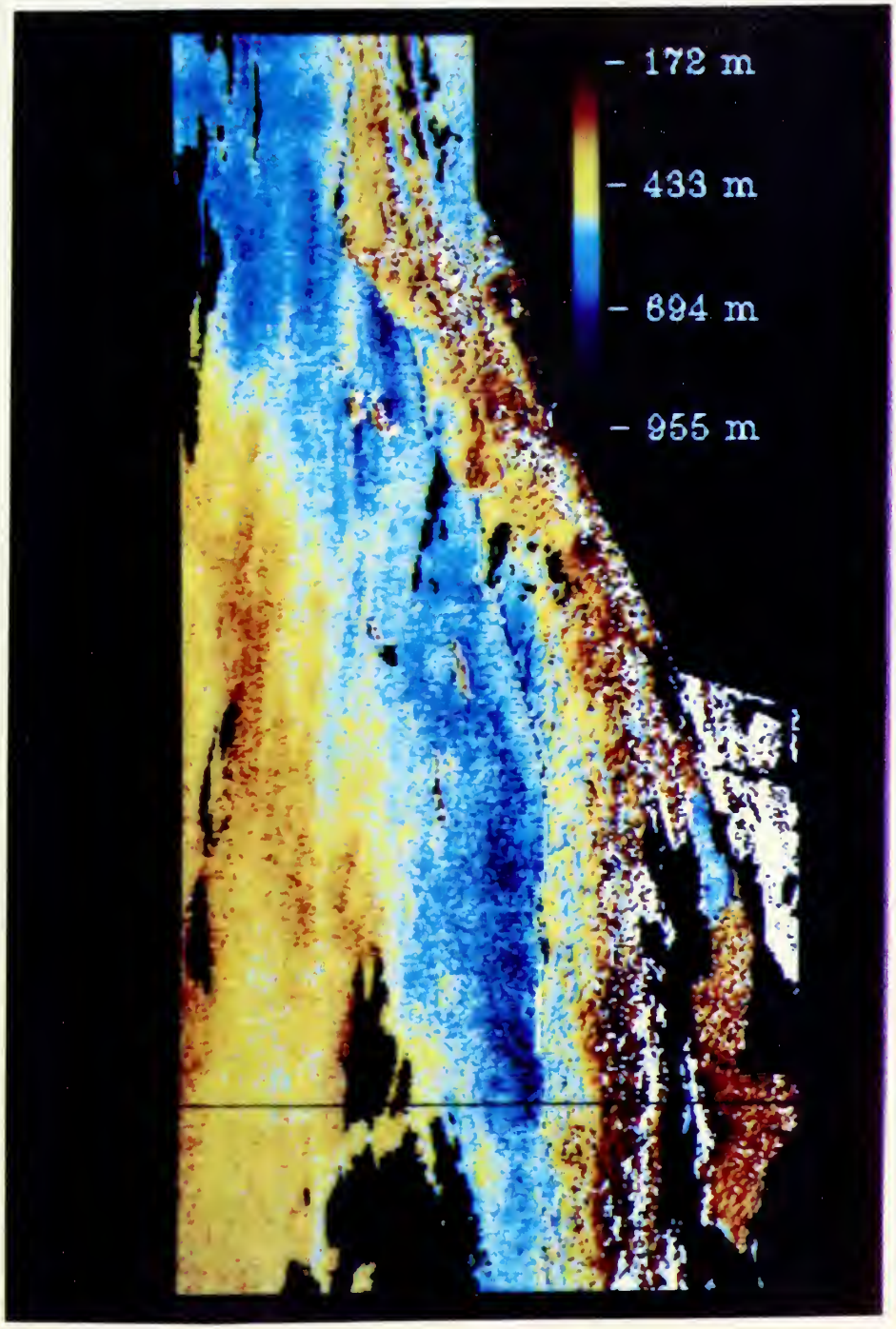

Fig. 24. Boundary layer depth image from 5 October 1982

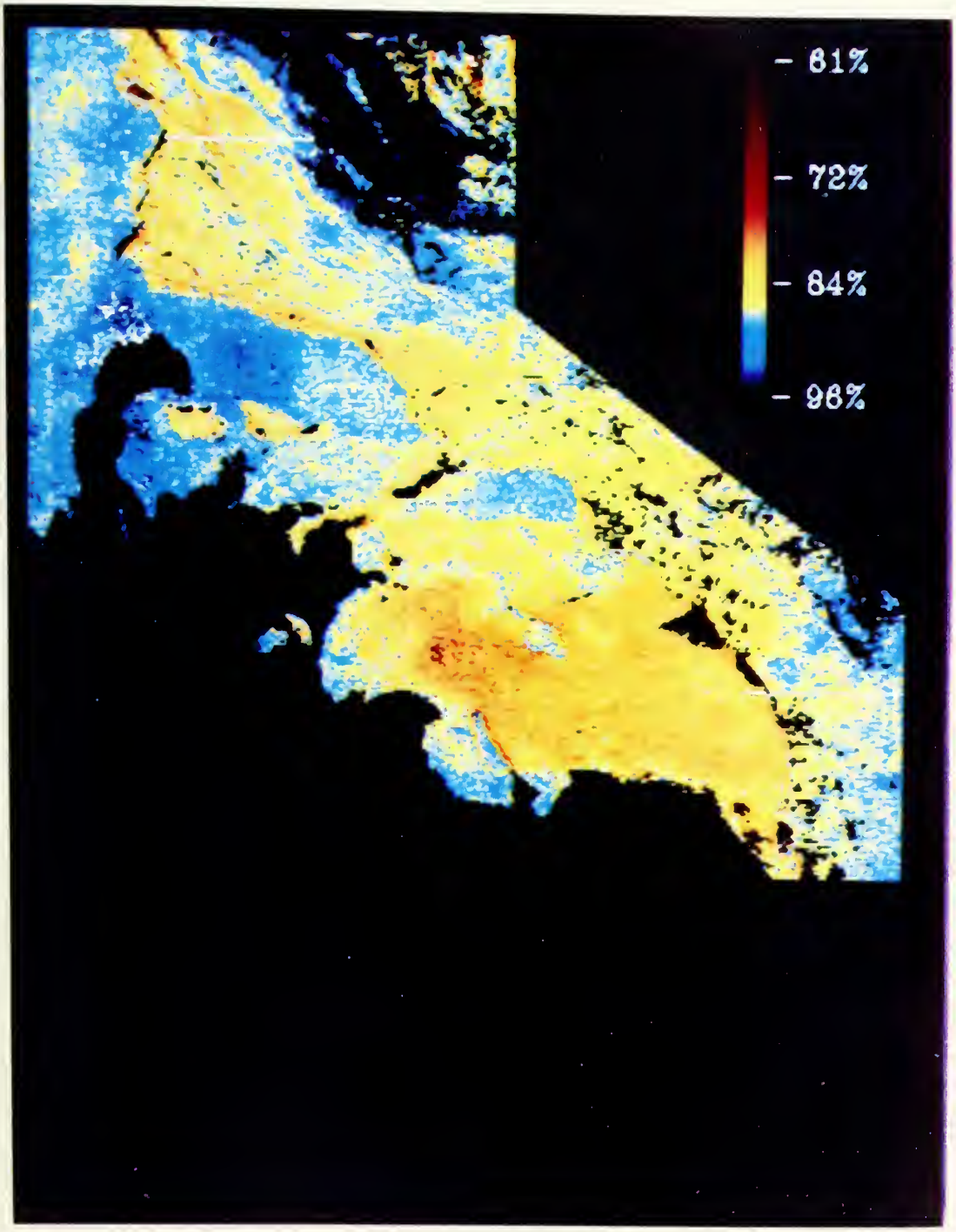

Fig. 25. Surface relative humidity image from 7 July 1987

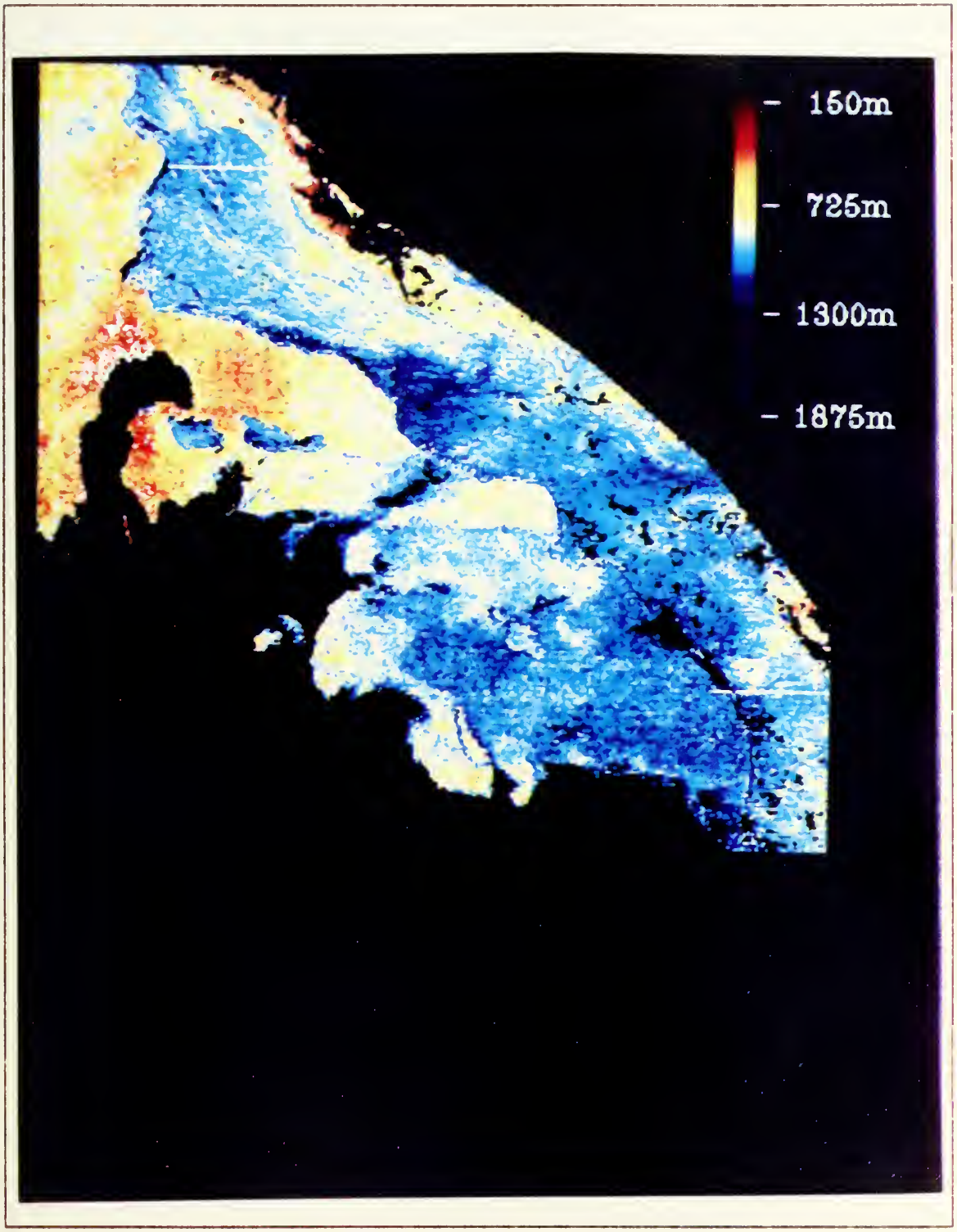

Fig. 26. Boundary layer depth image from 7 July 1987

from the California coast again probably played a part in driving down the surface relative humidity values. The colder sea-surface temperatures to the north produced corresponding higher surface relative humidities in the range of 92% to 95% since the near surface air would hold less moisture and thus have a lower saturation vapor density. This is also manifested in the boundary layer depth image for 7 July 1987 (Fig. 26), where generally the lower surface relative humidities around Santa Catalina correspond to high boundary layer depths of 1100 m to 1400 m.

For the 12 July 1987 cases, Figs. 27 and 28, a similar pattern to the 7 July 1987 case exists. High surface relative humidities, from 90% to 95%, are present in the colder, northern waters with the lower surface relative humidities hugging the coast below Point Conception. Surface relative humidities of 78% to 95% and boundary layer depths of 500 to 900 m exist around San Nicholas Island, consistent with the verified values presented in Chapter III.

D. FASINEX IMAGES OF 23 FEBRUARY 1986

The final set of images was taken from the Frontal Air-Sea Interaction Experiment (FASINEX) data set of 13 February to 10 March 1986 conducted in the Atlantic sub tropical convergence zone. Fig. 29 shows the satellite subscene region and synoptic situation for 23 February 1986, the day the images were produced, (Fellbaum et. al., 1986). Fig. 30 and Fig. 31 are the surface relative humidity and boundary layer depth images for the FASINEX cases respectively, centered on 28° N and 75° W. The horizontal white lines in the images define unuseable satellite data, as in the October 1982 cases.

The synoptic situation was similar to the coastal California cases, with a high pressure system dominating the weather for the period. This set of images was not able to be verified because of a disparity between the satellite pass and the ship location. The easternmost point of the satellite pass was at 72° W while the ship on 23 February was located at 69° W. Nevertheless, the two images represent an application of the technique in a different region of the world from the verified cases off the coast of California.

The images contain average surface relative humidities (70%) significantly lower and average boundary layer depths (1200 m) significantly deeper than the coastal California average values of 82% and 650 m respectively. Even though true verification could not be accomplished, the average values for the FASINEX images correspond with the radiosonde launches of 23 February by the R/V Endeavor. For surface relative humidity, the average satellite estimated value was 70% as compared to the Endeavor's

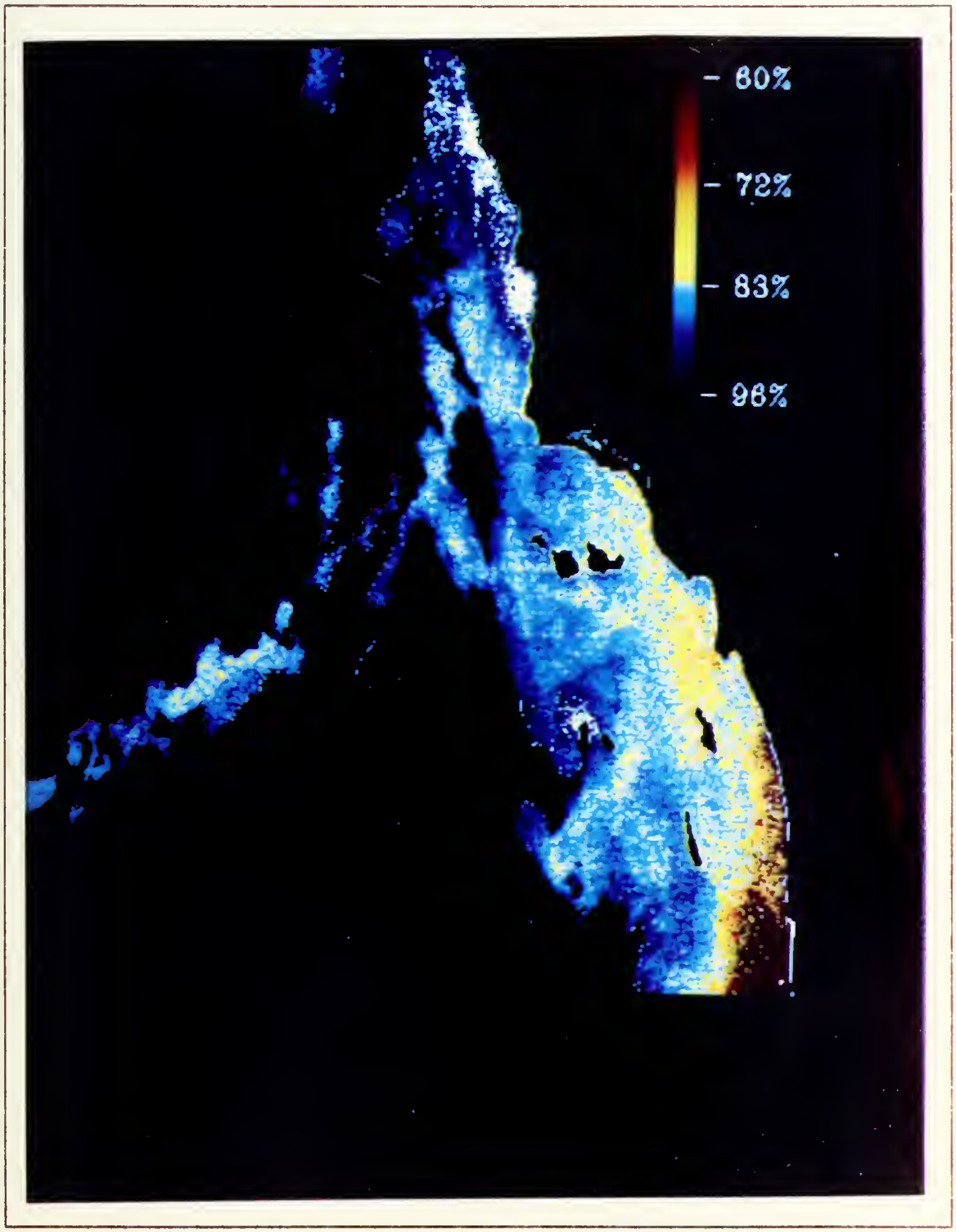

Fig. 27. Surface relative humidity image from 12 July 1987

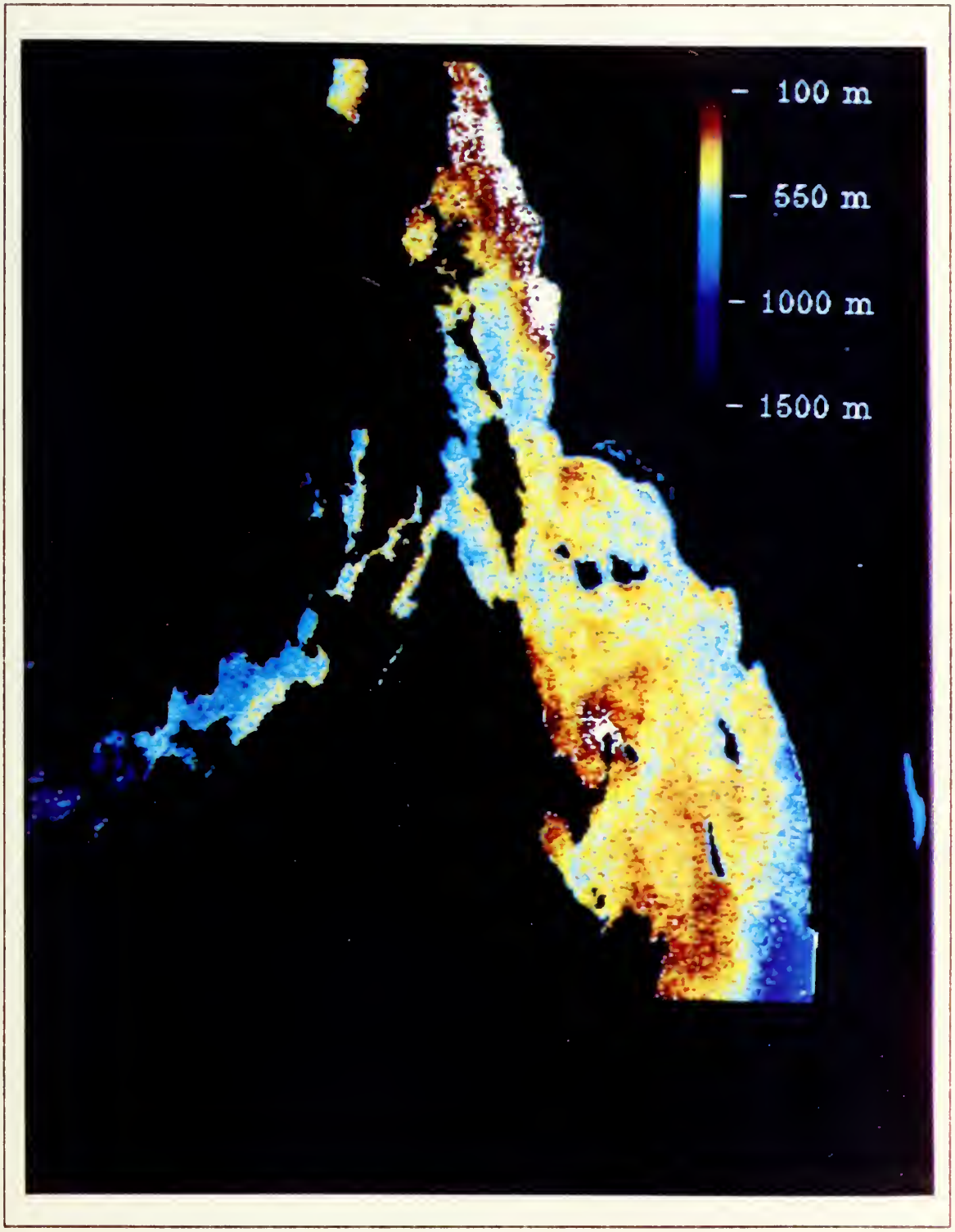

Fig. 28. Boundary layer depth image from 12 July 1987

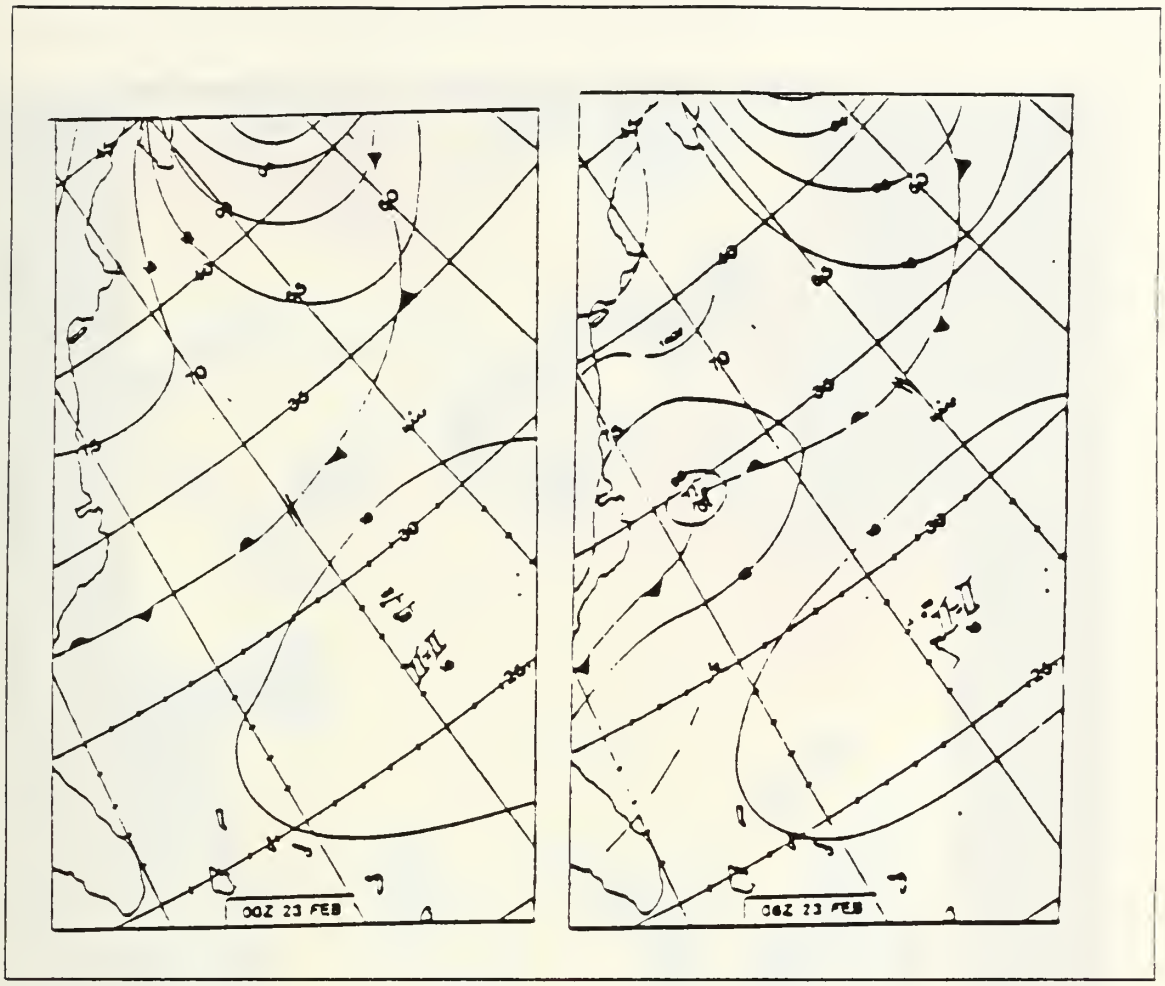

Fig. 29. FASINEX region and synoptic condition for 23 February 1986.

report of 67%. For boundary layer depth, the average satellite estimate was 1400 m as compared with the endeavor value of 1850 m.

The atmospheric variables of surface relative humidity and boundary layer depth would be less likely to vary over a large range in open ocean conditions as opposed to a coastal environment. The relatively close correlation between the satellite estimated measurements and the radiosonde reports of 23 February 1986 help to show the technique is applicable to more than a single geographic location. Further verification tests are necessary to solidify the usefulness of the technique not only in differing geographic locations but under varying synoptic situations as well.

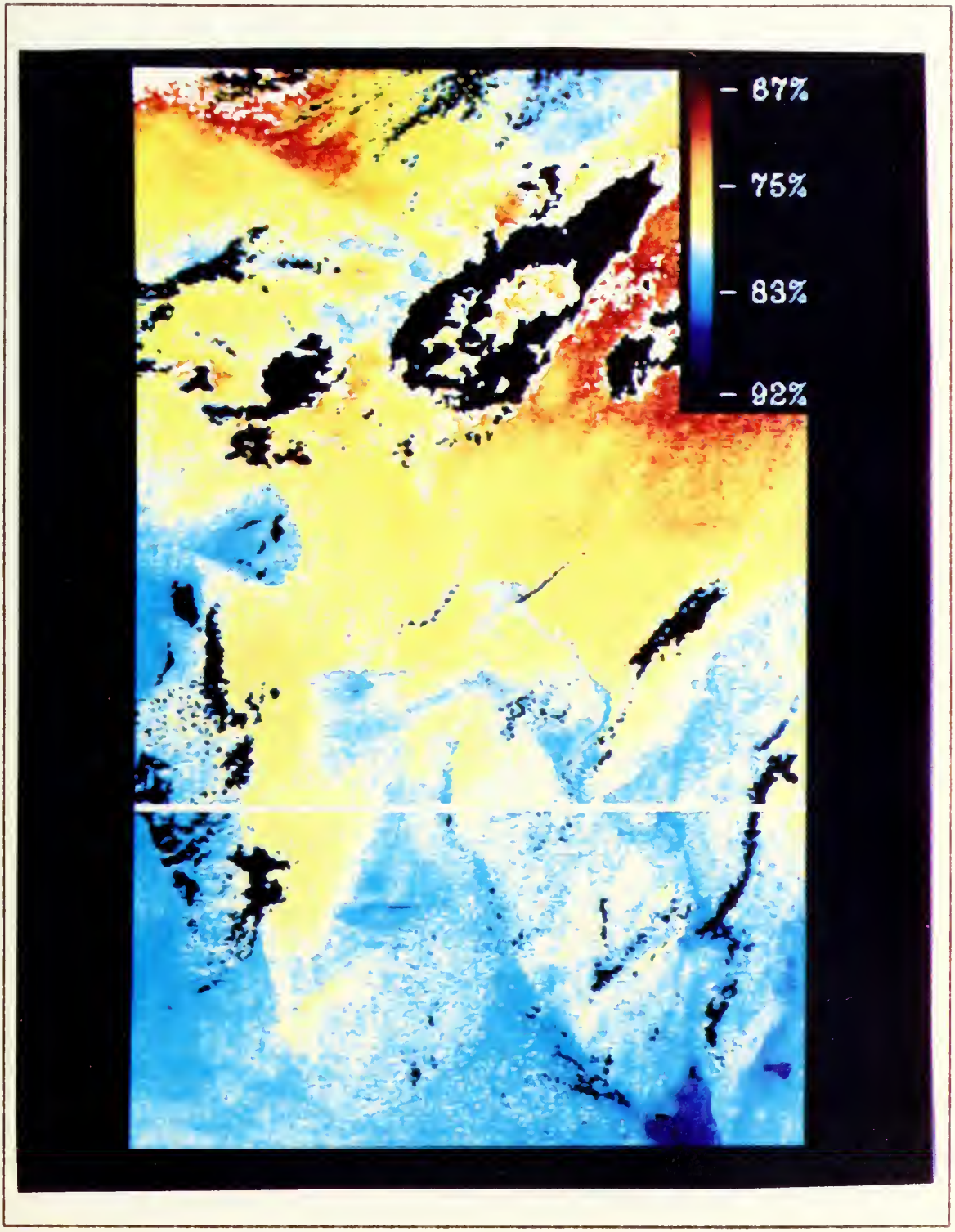

Fig. 30. Surface relative humidity image from 23 February 1986.

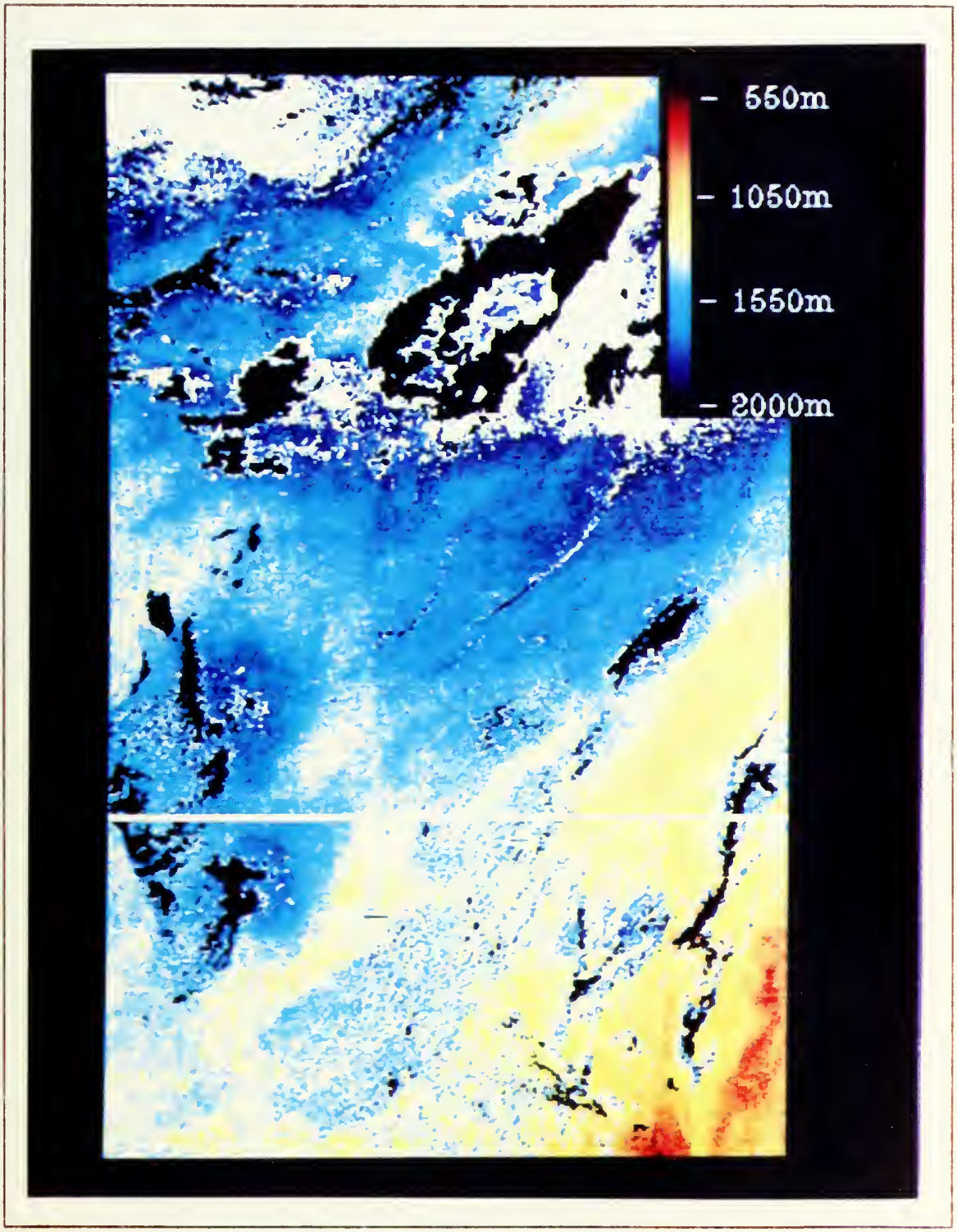

Fig. 31. Boundary layer depth image from 23 February 1986.

V. CONCLUSIONS AND RECOMMENDATIONS

The technique developed by Kren (1987) to estimate surface relative humidity and MABL depth from multispectral satellite measurements was proven to be theoretically feasible using simulated conditions and model atmospheres. The purpose of this thesis was to:

1. Test the response of the technique of combined AVHRR sensor measurement errors of sea-surface temperature, optical depth and total water vapor to the outputs of surface relative humidity and boundary layer depth under simulated conditions.

2. Compare satellite measured estimations of sea-surface temperature, optical depth, total water vapor, and derived estimations of surface relative humidity and boundary layer depth to verified values.

3. Incorporate the technique into an image processing algorithm that maps the surface relative humidity and boundary layer depth fields on a synoptic scale.

The sensitivity study presented in Chapter II quantified the effect of combined measurement errors under several different simulated boundary layers. The standard deviations for surface relative humidity cases ranged from 2.1% to 6.3%. The standard deviations for boundary layer depth cases ranged from 94.9 m to 168.6 m. Errors in the estimates of surface relative humidity and boundary layer depth tended to increase as the surface relative humidity decreased. There was little change in the estimates of surface relative humidity and boundary layer depth as a result of changes in sea-surface temperature.

Chapter III highlighted the results of the verification study comparing satellite data to verified measurements of sea-surface temperature, total water vapor and optical depth. The standard deviations between the satellite estimates and the verified measurements for surface relative humidity and boundary layer depth were 6% and 75m respectively.

A significant bias exists in the technique to estimate surface relative humidity. The tendency is to overestimate the correct value because a portion of the total water vapor exists above the boundary layer. This deviation from the initial assumptions resulted in overestimates of the surface relative humidity in nine of ten verification cases.

In Chapter IV, color enhanced images of sea-surface temperature, total water vapor, optical depth, surface relative humidity and boundary layer depth were presented for a variety of times and geographic locations. The horizontal variability in the surface

relative humidity and boundary layer depth fields on a synoptic scale was observable in all of the cases presented.

The images produced in this thesis represent the first attempt at mapping the surface relative humidity field and boundary layer depth field from satellite derived measurements of sea-surface temperature, total water vapor and optical depth. Several areas of study remain to refine the technique for use in boundary layer research and prediction.

First, implement a recently developed water vapor retrieval method from the AVHRR sensor that accounts for water vapor above the boundary layer. In this way a more accurate estimate of the most sensitive of input variables, total water vapor, can be implemented into the technique. It is possible that the technique is sensitive to variations in moisture above the boundary layer such that these variations directly influence the surface relative humidity value. Knowledge of the distribution of total water vapor derived from AVHRR sensor measurements would help determine if a relationship between upper level moisture and surface relative humidity exists.

Second, test the imaging technique under a variety of synoptic situations and geographic locations. Theoretically, the technique is constrained to regions of strong subsidence inversions away from continental aerosol influence. Subsidence inversions can also be associated with stable boundary layers which do not meet the well-mixed assumption. The validity of the technique in these and other synoptic conditions has yet to be determined. Also, the verification presented here was limited to a single geographic region. Further verification in other regions of the world is necessary to test the overall effectiveness of the technique.

Third, investigate the incorporation of the technique into dynamic numerical weather prediction (NWP) models. Real time horizontal variability of the MABL on a synoptic scale does not presently exist, and this information could aid the ability of NWP models to more accurately predict near-surface conditions.

Presently, the MABL is the region in the atmosphere most difficult to glean information from using remote sensing techniques. The broad nature of the weighting function associated with satellite based atmospheric sounders does not allow for sufficient vertical resolution to detect moisture content and temperature in the boundary layer. The method developed by Kren (1987) and advanced in this thesis uses a unique and previously untried approach to extract information about the boundary layer. Further

refinement of the technique is necessary in order for it to be used on a universal basis under real time conditions.

REFERENCES

Bolton, D., 1980: The Computation of Equivalent Potential Temperature. *Monthly Weather Review,* **108** , 1046-1053.

Businger, J.A., 1985: The Marine Boundary Layer, from Air-Sea Interface to Inversion. *NCAR Technical Note 252,* National Center For Atmospheric Research Boulder, CO, 84 pp.

Dalu, G., 1986: Satellite Remote Sensing of Atmospheric Water Vapor. *International Journal of Remote Sensing*, **7** , 1087-1097.

Durkee, P.A., 1984: The Relationship Between Marine Aerosol Particles and Satellite-Detected Radiance. Ph.D. Dissertation, Colorado State University, Fort Collins, CO, 124 pp.

Fitzgerald, J.W., 1979: On the Growth of Aerosol Particles with Relative Humidity. NRL memo. report 3847. Naval Research Laboratory, Washington D.C.

Fellbaum, S.R., S. Borrman, P. Boyle, K. Davidson, W. Large, T. Neta and C. Vaucher, 1988: Frontal Air-Sea Interaction Experiment (FASINEX) Shipboard Meteorology and Weather Atlas. NPS-63-88-002, Naval Postgraduate School, Monterey, CA.

Jensen, D. R., P. Jeck, G. Trusty, and G. Schacher, 1980: Intercomparison of PMS Particle Size Spectrometers. Technical Report 555, Naval Ocean Systems Center, San Diego, CA.

Koepke, P., and H. Quenzel, 1981: Turbidity of the Atmosphere Determined by Satellite: Calculation of Optimum Viewing Geometry. *Journal of Geophysical Research,* **84,** 7487-7856.

Kren, R.J., 1987: Estimation of Marine Boundary Layer Depth and Relative Humidity with Multispectral Satellite Measurements. M.S. Thesis, Naval Postgraduate School, Monterey, CA, 70 pp.

Lauritson, L., G. Nelson and F. Porto, 1979: Data Extraction and Calibration of TIROS-N NOAA Radiometers. NOAA Technical Memorandum NESS 107, National Oceanic and Atmospheric Administration, Washington D.C., 79 pp.

Liou, K.N., 1980: *An Introduction to Atmospheric Radiation*. Academic Press, New York, 392 pp.

McClain, P., 1985: Comparative Performance of AVHRR-Based Multichannel Sea Surface Temperature. *Journal of Geophysical Research*, **9**, 11,587-11,601.

McMillin, L.M., and D.S. Crosby, 1984: Theory and Validation of the Multiple Window Sea Surface Temperature Technique. *Journal of Geophysical Research*, **89**, 3655-3661.

Nieman, R.A., 1977: A Comparison of Radiosonde Temperature and Humidity Profile Data Bases, CSC TM-77 6133, Contract NAS 5 -11999, Computer Sciences Corp., Silver Spring, MD, 48 pp.

Rogers, R.R., 1979: *A Short Course in Cloud Physics*, Pergamon Press, New York, 235 pp.

Shettle, E.P., and R.W. Fenn, 1979: Models for the Aerosols of the Lower Atmosphere and the Effects of Humidity Variations on their Optical Properties. AFGL-TR-79-0214, Air Force Geophysics Laboratories, Hanscom AFB, MA, 94 pp.

INITIAL DISTRIBUTION LIST

		No. Copies
1.	Defense Technical Information Center Cameron Station Alexandria, VA 22304-6145	2
2.	Library, Code 0142 Naval Postgraduate School Monterey, CA 93943-5002	2
3.	Chairman Code 63Rd Department of Meteorology Naval Postgraduate School Monterey, CA 93943-5000	1
4.	Professor Philip A. Durkee Naval Postgraduate School Monterey, CA 93943-5000	1
5.	Chairman Code 68Co Department of Oceanography Naval Postgraduate School Monterey, CA 93943-5000	1
6.	Commander Naval Oceanography Command NSTL Station Bay St. Louis, MS 39522	1
7.	Commanding Officer Fleet Numerical Oceanography Center Monterey, CA 93943-5005	1
8.	Commanding Officer Naval Environmental Prediction Research Facility Monterey, CA 93943-5006	1
9.	Chairman, Oceanography Department U. S. Naval Academy Annapolis, MD 21402	1

Thesis
S635 Smolinski
c.1 Marine boundary layer depth and relative humidity estimates using multispectral satellite measurements.

Marine boundary layer depth and relative

3 2768 000 78944 0
DUDLEY KNOX LIBRARY.